Cell Reports

Article

Context-restricted PD-(L)1 checkpoint agonism by CTLA4-Ig therapies inhibits T cell activity

Graphical abstract

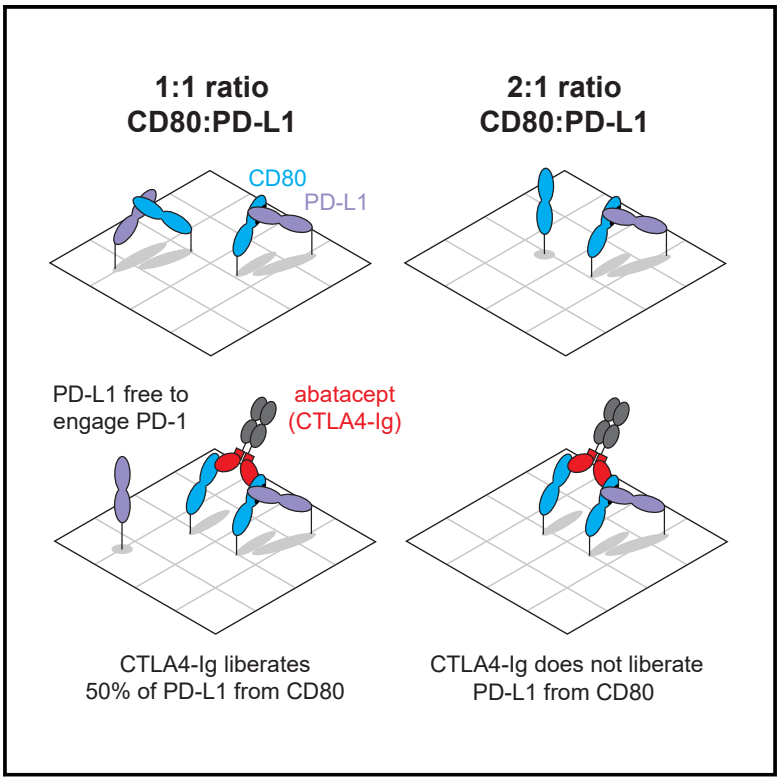

Authors

Ethan P. Oxley, Nadia J. Kershaw, Cynthia Louis, ..., Nicholas D. Huntington, Ian P. Wicks, Ross A. Dickins

Correspondence

ross.dickins@monash.edu

In brief

CTLA4-Ig therapies, including abatacept, are widely used in autoimmune and inflammatory disease. Oxley et al. identify the specific contexts where CTLA4-Ig binding to cell surface CD80 can release the immune inhibitory protein PD-L1. This extends the known mechanism of action of CTLA4-Ig therapies with implications for their rational clinical use.

Highlights

- CD80 reorientation by CTLA4-Ig liberates PD-L1
- CTLA4-Ig releases PD-L1 at CD80:PD-L1 ratios up to 2:1
- At best, CTLA4-Ig releases only half of total surface PD-L1 from CD80
- PD-(L)1 checkpoint agonism by CTLA4-Ig can contribute to T cell inhibition

Oxley et al., 2024, Cell Reports *43*, 114834
October 22, 2024
https://doi.org/10.1016/j.celrep.2024.114834

CellPress

Cell Reports

CellPress
OPEN ACCESS

Article

Context-restricted PD-(L)1 checkpoint agonism by CTLA4-Ig therapies inhibits T cell activity

Ethan P. Oxley,[1,11] Nadia J. Kershaw,[2,3,11] Cynthia Louis,[2,3] Katharine J. Goodall,[1] Maximilian M. Garwood,[1] Skye Min Jee Ho,[1] Veronica T.F. Voo,[1] Hae-Young Park,[4] Josephine Iaria,[2] Lilian L.L. Wong,[2] Ariel G. Lebenbaum,[1] Stephanie Wiranata,[1] Ee Shan Pang,[4] Emily S.J. Edwards,[5] Damian B. D'Silva,[2] Jacinta Hansen,[2] Menno C. van Zelm,[5,6] Meredith O'Keeffe,[4] P. Mark Hogarth,[7,8] Nicole M. Haynes,[9,10] Nicholas D. Huntington,[4] Ian P. Wicks,[2,3] and Ross A. Dickins[1,12,*]

[1]Australian Centre for Blood Diseases, Monash University, 99 Commercial Road, Melbourne, VIC 3004, Australia
[2]Walter and Eliza Hall Institute of Medical Research, 1G Royal Parade, Parkville, VIC 3052, Australia
[3]Department of Medical Biology, The University of Melbourne, Royal Parade, Parkville, VIC 3052, Australia
[4]Biochemistry and Molecular Biology, Monash Biomedicine Discovery Institute, Monash University, Clayton, VIC 3800, Australia
[5]Department of Immunology and Pathology, Monash University, 99 Commercial Road, Melbourne, VIC 3004, Australia
[6]Department of Allergy, Immunology & Respiratory Medicine, Monash University, Melbourne, VIC 3004, Australia
[7]Burnet Institute, 85 Commercial Road, Melbourne, VIC 3004, Australia
[8]Department of Clinical Pathology, The University of Melbourne, Royal Parade, Parkville, VIC 3052, Australia
[9]Division of Cancer Research, Peter MacCallum Cancer Centre, Melbourne, VIC, Australia
[10]Sir Peter MacCallum Department of Oncology, The University of Melbourne, Parkville VIC 3052, Australia
[11]These authors contributed equally
[12]Lead contact
*Correspondence: ross.dickins@monash.edu
https://doi.org/10.1016/j.celrep.2024.114834

SUMMARY

T cell surface CTLA4 sequesters the costimulatory ligands CD80 and CD86 on antigen-presenting cells (APCs) to prevent autoimmunity. Therapeutic immunosuppression by recombinant CTLA4-immunoglobulin (Ig) fusion proteins, including abatacept, is also attributed to CD80/CD86 blockade. Recent studies show that CTLA4-Ig binding to APC surface *cis*-CD80:PD-L1 complexes can release the inhibitory ligand PD-L1, but whether this contributes to T cell inhibition remains unclear. Here, we show that PD-L1 liberation by CTLA4-Ig is strictly limited, both in extent and context, relative to PD-L1-competing anti-CD80 antibodies. At APC surface CD80:PD-L1 ratios exceeding 2:1, CTLA4-Ig therapies fail to release PD-L1 regardless of their CD80 affinity. Additionally, introducing flexibility into CTLA4-Ig by modifying its rigid homodimer interface produces biologics that retain bivalent CD80 binding without dissociating *cis*-bound PD-L1. These findings demonstrate that CTLA4-Ig therapies liberate PD-L1 through a CD80 reorientation mechanism that imposes a strict context dependence to their PD-1 checkpoint agonism and resultant T cell inhibition.

INTRODUCTION

T cells are activated by sustained interactions with antigen-presenting cells (APCs) that trigger cognate antigen-dependent T cell receptor (TCR) signaling. Essential costimulatory signals are provided by the APC surface ligands CD80 (B7-1) and CD86 (B7-2), which bind the CD28 receptor on T cells. Conversely, the CTLA4 checkpoint limits T cell activity by sequestering these costimulatory ligands.[1] CTLA4 is a rigid-body transmembrane homodimer expressed on the surface of activated T cells.[2] While CD28 binding to APC surface CD80 and CD86 is monovalent and relatively weak, CTLA4 binding is bivalent and high avidity.[3–6] Hence, T cell surface CTLA4 inhibits T cell activity by outcompeting CD28 for its ligands.[3–5]

Abundant surface CTLA4 is a hallmark of regulatory T (Treg) cells, which restrain T cell responses to self-antigens. Upon APC engagement, Treg cell CTLA4 sequesters CD80 and CD86 and strips them from the APC surface through transendocytosis.[7,8] Reduced CTLA4 activity is associated with autoimmune disease,[9,10] and CTLA4-deficient mice develop fatal T cell-mediated multi-organ autoimmunity.[11,12] Accordingly, although CTLA4 checkpoint blockade with anti-CTLA4 antibodies such as ipilimumab can trigger potent anti-tumor T cell immunity,[13] it can also cause dose-limiting immune-related adverse events.[14]

Recombinant CTLA4-immunoglobulin (Ig) fusion proteins, comprising a covalent homodimer of the human CTLA4 ectodomain fused to a human IgG1 Fc domain, are widely used as immunosuppressive therapies.[2,15–17] Similar to endogenous transmembrane CTLA4, soluble CTLA4-Ig binds APC surface CD80/CD86 to block costimulation. The CTLA4-Ig protein abatacept is approved for rheumatoid arthritis, juvenile idiopathic arthritis, and psoriatic arthritis,[17–19] and the closely related CTLA4-Ig therapy belatacept is approved for kidney transplant

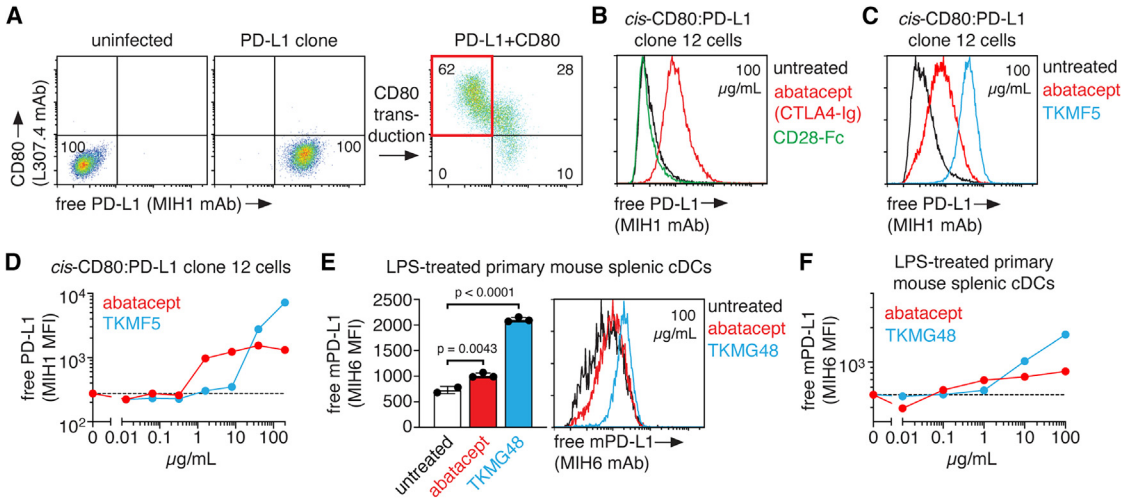

Figure 1. CTLA4-Ig releases PD-L1 from human and mouse *cis*-CD80:PD-L1 complexes

(A) Generating CHO cell clones co-expressing CD80 and PD-L1 but with low free PD-L1 (MIH1 mAb staining). The CD80^{high}PD-L1^{high}/MIH1^{low} gate from which *cis*-CD80:PD-L1 clones were sorted is shown in red.

(B) Free PD-L1 measured by MIH1 mAb staining of *cis*-CD80:PD-L1 clone 12 cells either untreated (black) or incubated with abatacept (red) or CD28-Fc (green).

(C) Free PD-L1 measured by MIH1 mAb staining of *cis*-CD80:PD-L1 clone 12 cells either untreated (black) or incubated with abatacept (red) or TKMF5 (blue).

(D) Abatacept and TKMF5 dose-response showing free PD-L1 (MIH1 mAb staining) on *cis*-CD80:PD-L1 clone 12 cells.

(E) Flow cytometry MFI (left) and histograms (right) of Cd11c^{+}major histocompatibility complex class II^{+} primary mouse conventional dendritic cells (cDCs) after 24 h LPS treatment, showing free mPD-L1 (MIH6) untreated or incubated with abatacept or TKMG48. Mean ± SD, $n = 2$ (untreated), $n = 3$ (abatacept, TKMG48), one-way ANOVA.

(F) Abatacept and TKMG48 dose-response showing free PD-L1 (MIH1 MFI) on LPS-treated primary mouse splenic cDCs.

rejection.[20,21] Although CTLA4-Ig therapies were first approved in 2005, additional disease indications continue to emerge. In 2021, abatacept was the first drug approved for prophylaxis of acute graft versus host disease following hematopoietic stem cell transplantation,[22] and in recent clinical trials, abatacept prevented or delayed onset of rheumatoid arthritis in at-risk individuals.[23,24] Based on recent promising findings in mouse models and cancer patients, abatacept is also in phase 3 clinical trials to alleviate acute myocarditis triggered by immune checkpoint inhibition.[25–27]

Another critical immunosuppressive checkpoint comprises the PD-1 surface receptor expressed on activated T cells and its ligands PD-L1 and PD-L2 expressed on cells including APCs. Liganded PD-1 inhibits T cell CD28 and TCR signaling,[28–31] and antibody blockade of PD-L1/PD-1 can trigger T cell-mediated antitumor immunity.[13,32] Recently CD80 and PD-L1 were found to bind each other in *cis* on the same APC surface.[33–35] The *cis*-CD80:PD-L1 interaction does not affect costimulatory CD80 *trans* binding to CD28 but prevents inhibitory PD-L1 *trans* binding to PD-1.[34,35] Hence, APC surface *cis*-CD80:PD-L1 complexes sequester PD-L1 to promote full T cell activation.[34–37] The therapeutic importance of *cis*-CD80:PD-L1 complexes was highlighted by a recent report describing anti-CD80 antibodies that release PD-L1 from CD80 by direct competition.[38] These antibodies bind CD80 at or close to its PD-L1 interface, opposite its CD28 binding site[39]; therefore, they still allow costimulation.[38] Nevertheless, these PD-1 agonist antibodies alleviate disease in several mouse models of autoimmunity.[38]

Several recent studies have examined the functional intersection between the *cis*-CD80:PD-L1 complex and CTLA4.[34,35,39–41] Mutagenesis and crystallography reveal that PD-L1 binds the homodimerization interface of CD80 opposite its CTLA4/CD28 binding site,[39,40] raising the possibility that CD80 may simultaneously bind PD-L1 in *cis* and CTLA4 in *trans*. However, in *in vitro* assays, *cis*-bound PD-L1 inhibits CD80 interactions with CTLA4.[35] Furthermore, a recent study shows that binding of CTLA4-Ig or Treg cell surface CTLA4 to mouse APC surface *cis*-CD80:PD-L1 complexes releases PD-L1.[41] A subsequent study also shows PD-L1 release from *cis*-CD80 upon Treg cell CTLA4-mediated transendocytic depletion of APC surface CD80/CD86, but CTLA4-Ig has little effect on levels of free PD-L1.[41,42] Despite some inconsistencies, these studies raise the possibility that CTLA4 may dampen T cell activation not only through blocking CD80/CD86 but also by releasing free PD-L1 on the APC surface. However, the biophysical mechanism of PD-L1 liberation by CTLA4-Ig is unknown, and it remains unclear whether this mechanism regulates T cell activity.[43]

RESULTS

Limited PD-L1 liberation from *cis*-CD80:PD-L1 complexes by abatacept (CTLA4-Ig)

To generate a platform for examining cell surface human *cis*-CD80:PD-L1 complexes, we first retrovirally expressed PD-L1 in Chinese hamster ovary (CHO) cells and isolated a PD-L1^{high} clone (Figure 1A). Co-expression of CD80 led to *cis*-CD80:PD-L1 complex formation, as evidenced by reduced binding of the anti-PD-L1 monoclonal antibody MIH1, which detects free but not CD80-bound PD-L1[44–46] (Figures 1A and S1A). Single-cell sorting from co-transduced populations yielded several stable

"*cis*-CD80:PD-L1" clones where MIH1 staining correlated with binding of recombinant PD-1-Fc, consistent with previous reports that *cis*-CD80:PD-L1 complexes prevent *trans*-PD-L1:PD-1 binding[33–35] (Figures S1A and S1B).

Recombinant CD28-Fc and CTLA4-Ig (abatacept) are disulfide-linked homodimeric fusion proteins with ligand-binding properties resembling native membrane-bound CD28 and CTLA4.[3] Whereas CD28-Fc binding to *cis*-CD80:PD-L1 clone cells had no effect, clinical-grade abatacept reproducibly triggered significant PD-L1 liberation, as shown by closely correlated MIH1 or PD-1-Fc staining in independent *cis*-CD80:PD-L1 clones (Figures 1B and S1C–S1H). In co-culture experiments, abatacept significantly increased *cis*-CD80:PD-L1 clone 12 cell interactions with PD-1 cells, which could be reversed by the clinical checkpoint inhibitor nivolumab (anti-PD-1) (Figures S1I–S1L). Human CTLA4 binds mouse (m)CD80, and, accordingly, abatacept treatment of CHO cells co-expressing mCD80 and mPD-L1 also triggered mPD-L1 liberation, as indicated by PD-1-Fc binding and interactions with mPD-1 cells (Figures S2A–S2G). In contrast to previous reports,[46] we found that low concentrations of the anti-mPD-L1 antibody clone MIH6 can specifically detect free mPD-L1 (Figures S2H–S2L). By this measure, abatacept also liberated endogenous mPD-L1 from mCD80 in primary mouse dendritic cells (Figures S2K–S2N). These results build on previous observations in mouse APCs[41] in support of an evolutionarily conserved *cis* interaction between CD80 and PD-L1 that is susceptible to disruption by CTLA4-Ig.

A recent report described the anti-CD80 antibody TKMF5, which competitively displaces PD-L1 from CD80.[38] Treatment of *cis*-CD80:PD-L1 clone 12 cells with 100 μg/mL TKMF5 triggered superior PD-L1 liberation compared to abatacept/CTLA4-Ig (Figure 1C). In dose/response studies, abatacept released PD-L1 at concentrations as low as 1 μg/mL; however, this reached a maximum plateau beyond 10 μg/mL (which is below the effective serum concentration in rheumatoid arthritis patients[47]; Figure 1D). In contrast, under 10 μg/mL TKMF5 did not release PD-L1, but at higher concentrations, TKMF5 increased free PD-L1 and surpassed the effect of abatacept (Figure 1D).

We performed similar experiments in primary mouse dendritic cells using the anti-mCD80 antibody TKMG48, which competitively releases PD-L1, similar to TKMF5.[38] Once again, PD-L1 release by TKMG48 was superior to abatacept at high doses (Figures 1E and 1F). Hence, PD-L1 release by CTLA4-Ig therapies is sub-optimal relative to TKMF5/TKMG48.

Biophysical and structural models of PD-L1 liberation by CTLA4-Ig

A recent crystal structure of the *cis*-CD80:PD-L1 complex (PDB: 7TPS) shows that the PD-L1 IgV-like domain engages the homodimerization surface of CD80, which is opposite its CTLA4/CD28 binding face[39,40] (Figures 2A and 2D). The CD80-binding surface of PD-L1 also partially overlaps its binding site for PD-1 and the anti-PD-L1 antibodies atezolizumab and durvalumab[39,48–50] (Figure S3A), consistent with functional sequestering of PD-L1 by CD80, as observed by us and others.[33,35,37,40] Since the structured ectodomains of CD80 and PD-L1 are both ~90 Å long and similarly shaped, with 9- and 11-residue membrane-tethered stalks, respectively,[4,48,49] the ~65° *cis* interaction angle observed in the crystal structure tilts them toward each other and oblique to the membrane (Figure 2A). In contrast, two CD80 molecules bivalently crosslinked by homodimeric CTLA4 adopt a parallel configuration in crystal structures (PDB: 1I8L)[4] (Figures 2B and 2C). Superimposing these structures and assuming minimal close-range membrane curvature, a rigid CTLA4 homodimer cannot bivalently bind two membrane-bound *cis*-CD80:PD-L1 duplexes (Figure S3B).

This structural analysis suggests two potential mechanisms by which a CTLA4-Ig homodimer could release PD-L1 from *cis*-CD80. In the first scenario, bivalent CTLA4-Ig binding reorients one CD80 molecule, thus releasing a single PD-L1 molecule, while the other *cis*-CD80:PD-L1 complex remains intact (Figures 2B and 2E; Video S1). This model, designated "half-liberation," predicts limitations on both the extent of PD-L1 liberation by CTLA4-Ig and the contexts where it occurs. It predicts peak PD-L1 liberation by CTLA4-Ig at CD80:PD-L1 ratios around 1:1; however, even then, only half of the PD-L1 molecules on the cell surface are released, and the other half remain sequestered in *cis*-CD80:PD-L1 duplexes (Figures 2F and S3C). Importantly, according to the half-liberation model, CTLA4-Ig binding does not release any PD-L1 at cell surface CD80:PD-L1 ratios of 2:1 or more (Figures 2F and S3C).

In the second scenario, bivalent binding of CTLA4-Ig brings both CD80 molecules into a membrane-perpendicular upright position, thus releasing two PD-L1 molecules (Figures 2C and 2G; Video S2). By this "full liberation" model, CTLA4-Ig releases all PD-L1 molecules regardless of CD80:PD-L1 ratio (Figures 2I and S3C). Notably, the anti-CD80 antibody TKMF5, which competitively displaces PD-L1 from CD80,[38] is similarly predicted to release all PD-L1 molecules (Figures 2H and S3C).

Both CTLA4-Ig bivalent binding models involve reorientation of at least one CD80 molecule so it can no longer bind membrane-tethered PD-L1. However, this reoriented CD80 is predicted to still bind soluble, untethered PD-L1. Consistent with this possibility, CTLA4-Ig treatment of *cis*-CD80:PD-L1 clone cells promoted simultaneous binding of a soluble PD-L1-Fc fusion protein (Figure S3D).

PD-L1 liberation by CTLA4-Ig is limited, and cell surface CD80:PD-L1 ratio dependent

To determine whether CTLA4-Ig triggers PD-L1 half-liberation or full liberation, we generated a CHO cell line co-transduced with two retroviral vectors: one encoding CD80 fused to intracellular monomeric Cherry (mCherry) and another encoding PD-L1 fused to intracellular monomeric green fluorescent protein (mGFP) (Figure S4A). This population of co-transduced cells has an mCherry:mGFP fluorescence ratio reflecting relative surface CD80:PD-L1 expression. Indeed, across cells with similar mid-range PD-L1mGFP expression, free surface PD-L1 was readily detected on CD80mCherry^{LOW} cells but fell to background levels in CD80mCherry^{HIGH} cells, consistent with *cis*-CD80:PD-L1 complex formation (Figure 3A). Assuming similar infection efficiency and fusion protein production from the CD80mCherry and PD-L1mGFP vectors, we adjusted flow cytometry detection parameters so the mean fluorescence intensity (MFI) of mCherry approximately matched mGFP MFI within the co-transduced

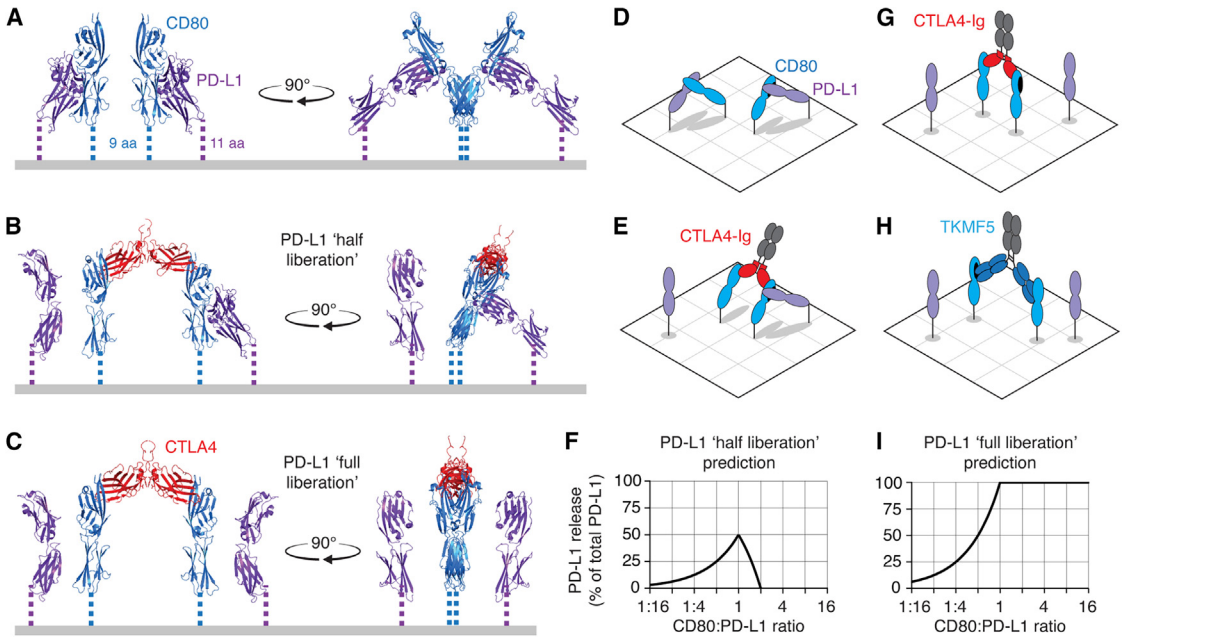

Figure 2. Structure-based models of CTLA4-Ig binding to *cis*-CD80:PD-L1 complexes

(A) Model of two cell surface *cis*-CD80:PD-L1 duplexes based on crystal structures.[39] Membrane-tethered stalk regions are modeled as dotted lines to approximate scale.

(B and C) Models of PD-L1 half-liberation (B) or full liberation (C) from *cis*-CD80 by CTLA4-Ig based on crystal structures.[4,39]

(D and E) Cartoons of (A) and (B), respectively. The PD-L1 binding site on CD80, which is similar to the CD80 homodimerization interface, is shown in black.

(F) Theoretical PD-L1 release (proportion of total PD-L1) at different CD80:PD-L1 surface ratios predicted by the half-liberation model.

(G) Cartoon of (C).

(H) Cartoon of PD-L1 full liberation from *cis*-CD80 by the anti-CD80 antibody TKMF5, which competitively displaces PD-L1 from CD80.[38]

(I) Theoretical PD-L1 release (proportion of total PD-L1) at different CD80:PD-L1 surface ratios predicted by the full liberation model.

population (Figures 3A, 3B, and S4B). Analysis of ~250,000 co-transduced cells revealed CD80mCherry:PD-L1mGFP ratios ranging from ~1:8 to ~8:1, and grouping cells within defined ratio ranges revealed a near-symmetrical distribution centered around 1:1 (Figures 3B and S4B). Binding of abatacept and atezolizumab to CD80 and total PD-L1, respectively, was closely correlated with the CD80mCherry:PD-L1mGFP fluorescence ratio of each cell, validating functional cell surface expression (Figure S4C). Population-wide analysis again showed abundant free PD-L1 at low CD80mCherry:PD-L1mGFP ratios, falling to background levels at ratios of 1:1 or more (Figure 3D).

Notably, high concentrations of CTLA4-Ig/abatacept did not trigger population-wide PD-L1 liberation (Figures 3C, 3D, and S4D). Abatacept liberated PD-L1 in cells with CD80mCherry:PD-L1mGFP ratios up to ~2:1 but had no effect at ratios above 2:1 regardless of absolute CD80mCherry and PD-L1mGFP expression (Figures 3D and S4E). Calculating abatacept-induced PD-L1 liberation as fold change relative to no treatment revealed an observed profile (Figure 3D, bottom) resembling the theoretical profile predicted by the PD-L1 half-liberation model (Figure 2F), where a single CTLA4-Ig homodimer disrupts one *cis*-CD80:PD-L1 duplex by crosslinking one "free" CD80 molecule and one PD-L1-bound CD80 molecule (Figures 2B and 2E; Video S1). In contrast, high-concentration TKMF5 liberated PD-L1 more effectively than CTLA4-Ig across a wider range of CD80mCherry:PD-L1mGFP ratios (Figures 3C, 3D, and S4D), consistent with competitive PD-L1 full liberation (Figures 2H and 2I). Similar results were obtained in replicate experiments (Figure S4F).

Using CD80mCherry:PD-L1mGFP cultures, we then performed dose-response studies comparing PD-L1 agonism by TKMF5, abatacept, and a previously described CTLA4-Ig variant with >100-fold higher affinity for CD80 (MEDI5265; hereafter designated CTLA4^{HA}-Ig)[51] (Figures 3E and S4G). At low concentrations, CTLA4^{HA}-Ig released more PD-L1 per cell than abatacept, as anticipated (Figure 3E). However, PD-L1 liberation by high-concentration CTLA4-Ig/abatacept and CTLA4^{HA}-Ig was indistinguishable, occurring only on cells with a CD80mCherry:PD-L1mGFP expression ratio under ~2:1 (Figure 3E). Hence, in accordance with the PD-L1 half-liberation model, enhancing the CD80/86 affinity of CTLA4-Ig (exemplified by MEDI5265 and belatacept[20,51]) does not alter the strict context dependence of its PD-L1-liberating activity. This was further supported by analysis of CD80mCherry:PD-L1mGFP cell sub-populations gated on approximate expression ratios of 1:1 or 4:1 (open or closed arrowheads in Figure 3E). For 1:1 cells, PD-L1 release by abatacept and CTLA4^{HA}-Ig was dose dependent and converged on a defined maximal plateau at higher concentrations (Figure 3F), similar to *cis*-CD80:PD-L1 clone 12 cells (Figure 1D). In contrast, for 4:1 cells, neither CTLA4-Ig fusion liberated PD-L1, but TKMF5 did (Figure 3F).

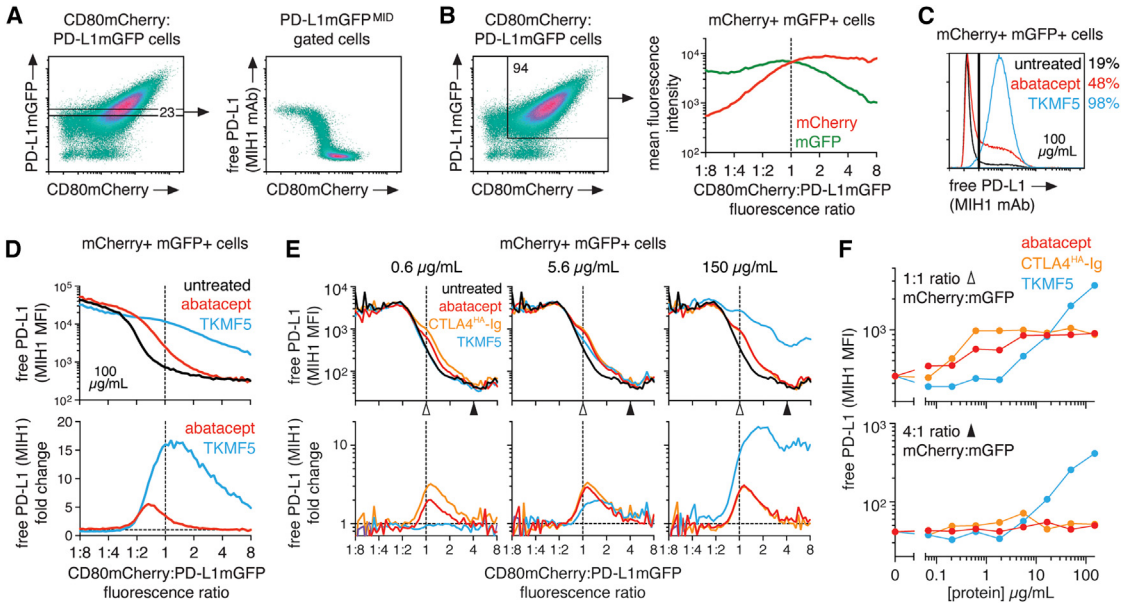

Figure 3. PD-L1 liberation by CTLA4-Ig depends on the surface CD80:PD-L1 ratio

(A) Flow cytometry of CHO cells co-transduced with CD80mCherry and PD-L1mGFP. For the indicated gated population (left), free PD-L1 (MIH1 staining) is plotted against CD80mCherry level (right).

(B) As for (A) but showing the CD80mCherry^{+}PD-L1mGFP^{+} population gated for export of individual MFI values (left). MFI data were used to generate a histogram with cells binned into equally spaced CD80mCherry:PD-L1mGFP MFI ratio intervals centered around 1:1. Average mCherry and mGFP MFI within each interval is shown (right).

(C) Free PD-L1 (MIH1 staining) profile of CD80mCherry^{+}PD-L1mGFP^{+} cells in (B), either untreated (black) or treated with abatacept (red) or TKMF5 (blue). Numbers indicate the percentage of MIH1^{+} cells within the gate for each condition.

(D) Top: average free PD-L1 (MIH1 MFI) across CD80mCherry:PD-L1mGFP ratio intervals of the cells in (B) when untreated or treated with abatacept or TKMF5. Bottom: the same data expressed as free PD-L1 fold change (relative to untreated) in response to abatacept and TKMF5.

(E) As in (D) for CD80mCherry^{+}PD-L1mGFP^{+} cells untreated (black) or treated with abatacept (red), high-affinity CTLA4-Ig (CTLA4^{HA}-Ig, orange), or TKMF5 (blue) at concentrations of 0.6 μg/mL, 5.6 μg/mL, and 150 μg/mL.

(F) Abatacept, CTLA4^{HA}-Ig, and TKMF5 dose-response showing free PD-L1 (MIH1 staining) on cells within the 1:1 (open arrowhead, top) and 4:1 (closed arrowhead, bottom) CD80mCherry:PD-L1mGFP ratios indicated in (E).

In further support of the PD-L1 half-liberation model, overexpressing CD80 in CD80mCherry:PD-L1mGFP cells impeded PD-L1 release by CTLA4-Ig (Figure S4H). Importantly, this was also seen in *cis*-CD80:PD-L1 clone 12 cells upon overexpression of CD86 or the CD80 mutants CD80^{I92R} and CD80^{L104D}, which do not *cis* bind PD-L1 (Figure S4I). Hence, by allowing bivalent CTLA4-Ig binding without *cis*-CD80:PD-L1 disassembly, excess CD80 or CD86 can indirectly reduce PD-L1 release (Figure S4J).

Together, these results support half and full PD-L1 liberation by abatacept and TKMF5, respectively, and consequent tight limitations on the extent and context dependence of PD-L1 release by CTLA4-Ig therapies. Notably, despite these restrictions, abatacept releases endogenous surface PD-L1 on activated primary mouse dendritic cells (Figures 1E and 1F).

Context-dependent PD-L1 release by abatacept can contribute to T cell inhibition

To generate cell lines with defined CD80:PD-L1 ratios, we sorted single cells from CD80mCherry:PD-L1mGFP cultures and produced a series of clones with similar PD-L1mGFP levels but increasing CD80mCherry expression (Figures 4A, S5A, and S5B). Clone 1 expresses PD-L1mGFP alone and, accordingly, has the highest free PD-L1 (Figure 4B). For clones 2–7, the average CD80mCherry:PD-L1mGFP ratio increases incrementally from ~1:4 (clone 2) up to ~4:1 (clone 7) with corresponding stepwise reductions in free PD-L1 due to sequestration by CD80 (Figures 4B, S5A, and S5C). Consistent with Figure 3 cell population observations, PD-L1 liberation by abatacept depended on the surface CD80:PD-L1 ratio of each clone (Figures 4C, S5C, and S5D). In clone 5 cells, where CD80mCherry and PD-L1mGFP expression is approximately equal, abatacept and TKMF5 both triggered PD-L1 release from CD80 (Figures 4C and 4D). In contrast, in clone 7 cells, where CD80mCherry:PD-L1mGFP expression is ~4:1, abatacept failed to release PD-L1 despite dose-dependent activity of TKMF5 (Figures 4C and 4D).

To assess whether PD-L1 release/agonism contributes to T cell inhibition by CTLA4-Ig, we performed *in vitro* primary human T cell activation assays. CD80mCherry:PD-L1mGFP clones 1–7 were first converted into artificial APCs (aAPCs) through stable retroviral expression of a membrane-bound anti-CD3 single-chain antibody fragment (OKT3-scFv), which induces TCR signaling (Figures 4E and S5E). Culturing naive primary human T cells for 4 days in plates pre-seeded with these aAPCs triggered T cell activation driven by synergistic TCR signaling and costimulation and induced T cell surface PD-1 (Figures 4F and 4G). Pre-activated T cell cultures were then treated with

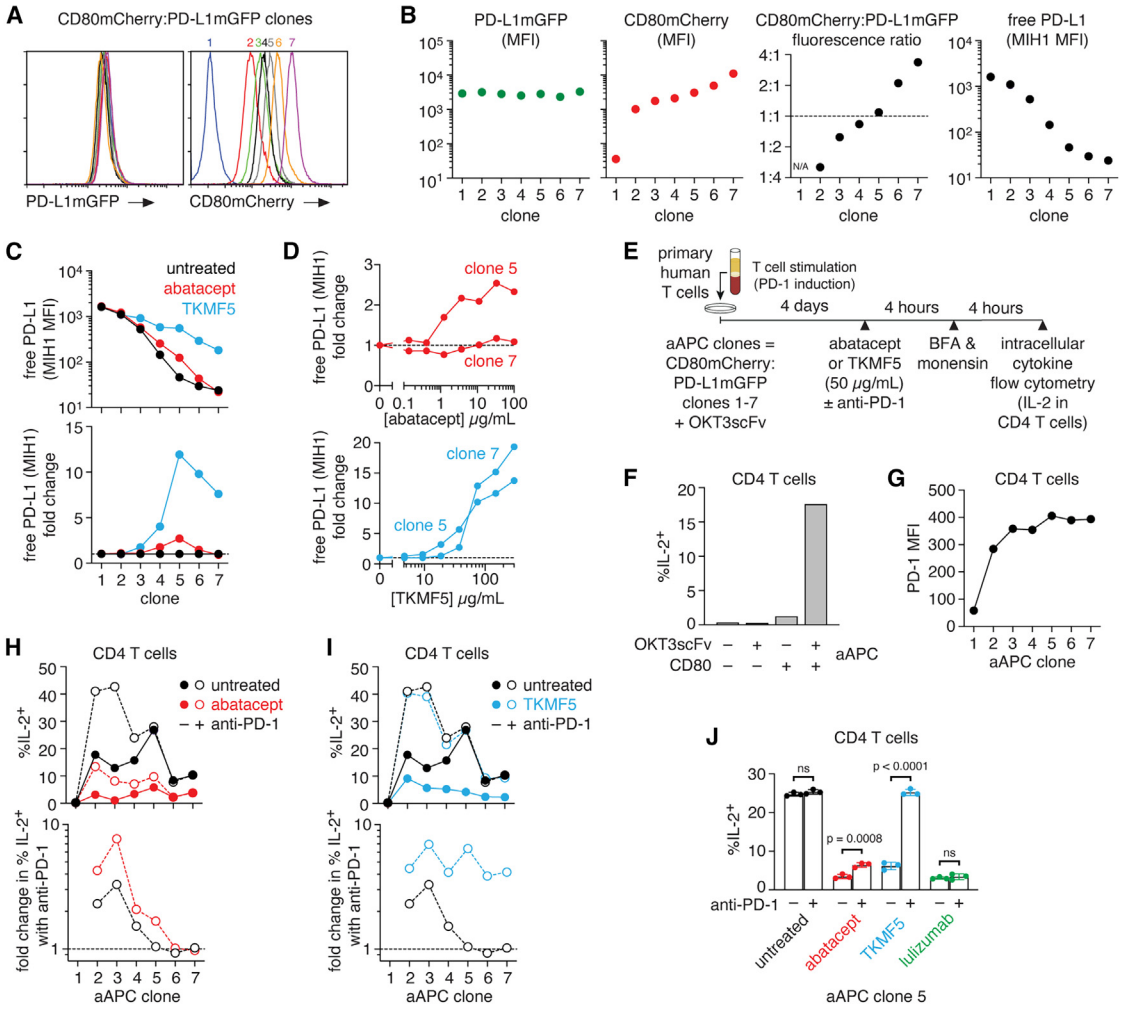

Figure 4. Context-dependent PD-(L)1 agonism by CTLA4-Ig

(A) Flow cytometry of PD-L1mGFP and CD80mCherry fluorescence in seven clones with equivalent PD-L1mGFP and increasing CD80mCherry expression.

(B) MFI of PD-L1mGFP (far left), CD80mCherry (center left), and free PD-L1 (MIH1 staining, far right) with corresponding CD80mCherry:PD-L1mGFP ratio (center right) for the seven CD80mCherry:PD-L1mGFP clones.

(C) Free PD-L1 (MIH1 MFI, top) and corresponding fold change (relative to untreated) of the seven CD80mCherry:PD-L1mGFP clones in response to abatacept and TKMF5.

(D) Abatacept (top) and TKMF5 (bottom) dose-response showing free PD-L1 in CD80mCherry:PD-L1mGFP clones 5 and 7.

(E) Schematic for pre-activated primary human T cell assay.

(F) Percent IL-2$^+$ primary human CD4 T cells cultured for 4 days with CHO cells expressing combinations of OKT3-scFv and/or CD80.

(G) PD-1 staining of CD4 T cells cultured for 4 days with the seven CD80mCherry:PD-L1 clones co-expressing OKT3-scFv (aAPC clones).

(H and I) Percentage of IL-2$^+$ CD4 T cells (top) cultured with the seven aAPC clones for 4 days, followed by 8 h incubation with or without abatacept (H) or TKMF5 (I). Dotted lines and open circles indicate co-treatment with anti-PD-1 (nivolumab), with the corresponding fold change in the percentage of IL-2$^+$ CD4 T cells by anti-PD-1 addition shown below.

(J) Percentage of IL-2$^+$ CD4 T cells following co-culture with aAPC clone 5 incubated with abatacept, TKMF5, or anti-CD28 scFv lulizumab with or without anti-PD-1 co-treatment. Mean ± SD, n = 3, one-way ANOVA.

biologics, and the CD4 T cell activation state was assessed by intracellular expression of the cytokine interleukin-2 (IL-2), shown previously to be PD-1 sensitive[52] (Figure 4E).

We initially verified PD-(L)1 checkpoint function in this assay using the anti-PD-1 antibody nivolumab. As anticipated, PD-1 blockade boosted T cell activity in cultures where aAPCs had free surface PD-L1 (clones 2–4) but not in aAPC clone 5–7 cultures, where PD-L1 is sequestered by CD80 (Figure 4H). Short-term treatment with abatacept/CTLA4-Ig alone potently suppressed T cell activity in all contexts (Figure 4H, top). This inhibition was unaffected by PD-1 blockade in aAPC clone 6 and 7 cultures, where the CD80:PD-L1 ratio exceeds 2:1, consistent with earlier biophysical data suggesting that abatacept does not engage the PD-(L)1 checkpoint in this context (Figure 4H). For aAPC clones 2–4, which display free PD-L1, PD-1 blockade partially reversed T cell inhibition by abatacept (Figure 4H). This

reversal could simply reflect anti-PD-1 single-agent effects. However, in aAPC clone 5 cultures, where surface CD80 and PD-L1 are approximately equal, PD-1 blockade partially reversed T cell inhibition by abatacept (approximately doubling the number of IL-2$^+$ T cells), but anti-PD-1 alone had no effect (Figures 4H and 4J). In the same context, the monovalent costimulation-blocking anti-human CD28 antibody lulizumab[53] reduced T cell activation to a similar extent as abatacept, but unlike abatacept, its effects were insensitive to PD-1 blockade (Figure 4J). These data indicate that PD-L1 release by CTLA4-Ig therapies can contribute to immunosuppression, but only in contexts where APC-surface CD80 and PD-L1 are similarly abundant. In the same assay, TKMF5 inhibited T cell activation regardless of aAPC surface CD80:PD-L1 ratio, in keeping with PD-L1 full liberation predictions (Figures 4I and 4J). TKMF5 effects were completed reversed by anti-PD-1, consistent with its sole activity as a PD-L1 liberator that does not block costimulation[38] (Figures 4I and 4J).

Monomeric CTLA4 binds CD80 without displacing PD-L1

CTLA4 has two endogenous isoforms: a transmembrane disulfide-linked homodimer and a secreted/soluble monomer (sCTLA4) that lacks the transmembrane domain[54] (Figure 5A). To examine monomeric CTLA4 interactions with surface *cis*-CD80:PD-L1, we fused sCTLA4 to a human IgG1 Fc domain harboring mutations that prevent dimerization[55] (MonoCTLA4-Ig). Control dimeric CTLA4-Ig (DimCTLA4-Ig) comprised the same monomeric Fc fused to the CTLA4 transmembrane isoform ectodomain, which includes Cys122 involved in covalent homodimerization[3,15] (Figures 5B and 5C). Recombinant MonoCTLA4-Ig and DimCTLA4-Ig behaved as monomers and dimers, respectively, by non-reducing SDS-PAGE (Figure S6A). Abatacept and DimCTLA4-Ig binding to *cis*-CD80:PD-L1 clone cells and CD80mCherry:PD-L1mGFP cultures triggered PD-L1 liberation, but MonoCTLA4-Ig did not, despite similar binding at saturating concentrations (250 μg/mL) (Figures 5D–5F and S6B). Consistent with structural modeling[4,6] (Figure 5G), our data demonstrate that monovalent biologics such as MonoCTLA4-Ig and CD28-Fc do not disrupt the *cis*-CD80:PD-L1 complex, whereas bivalent biologics, including abatacept and (Dim)CTLA4-Ig, release PD-L1 (Figure 5H).

Flexible CTLA4-Ig variants do not displace PD-L1 from CD80

Since monomeric CTLA4-Ig does not liberate PD-L1, we reasoned that dimeric CTLA4-Ig with longer "arms" may retain high-avidity bivalent CD80 binding without liberating PD-L1. To test this, we inserted flexible Gly/Ser linkers adjacent to the ligand-binding domains of CTLA4-Ig, displacing highly conserved CTLA4 residues (Asp118 to Pro121; DPEP) implicated previously in rigid-body homodimerization[2,56] (Figures 6A and S6C–S6E). These variants were termed Flex(n)CTLA4-Ig (with n = 30, 25, 20, 15, 10, 5, 3, 2, or 1 inserted Gly/Ser residues). Covalent homodimerization was maintained by CTLA4 stalk Cys122 and inclusion of two IgG1 hinge-region interchain disulfide Cys residues (mutated to Ser in abatacept[15]). Size-exclusion chromatography-multi-angle light scattering and non-reducing SDS-PAGE confirmed that FlexCTLA4-Ig proteins were not compromised by linker insertion and were produced as disulfide-linked homodimers of predicted molecular weight (Figure S6A and S6F–S6H).

In striking contrast to abatacept or otherwise identical control CTLA4-Ig, FlexCTLA4-Ig biologics failed to appreciably liberate PD-L1 despite similar binding to *cis*-CD80:PD-L1 cells (Figures 6B, 6C, and S6I–S6K). Similar results were obtained with CTLA4-Ig variants rendered flexible by substituting the conserved DPEP peptide within the stalk or by tethering two sCTLA4 monomers to an IgG Fc scaffold (FlexsCTLA4-Ig) (Figures S6L–S6N). For FlexCTLA4-Ig biologics with shorter linkers, we noted that some residual PD-L1-liberating activity was retained by Flex1CTLA4-Ig (a single Gly insertion), but this was reduced in Flex3CTLA4-Ig and disabled with linker lengths of 5 residues or more (Figures S7A and S7C). Similar observations were made using mouse primary splenic dendritic cells and CHO cells expressing *cis*-mCD80:mPD-L1 (Figures S7B and S7D–S7H). These data show that CTLA4-Ig rigidity is required for CD80 reorientation and PD-L1 release, in accordance with our structural models.

Bivalent binding of flexible CTLA4-Ig variants to *cis*-CD80:PD-L1 complexes

The binding profile of FlexCTLA4-Ig variants to *cis*-CD80:PD-L1 cells suggested an avid bivalent interaction (Figure 6C). As expected, Flex1CTLA4-Ig and parental CTLA4-Ig binding to *cis*-CD80:PD-L1 cells was significantly stronger than monomeric CTLA4-Ig, and both homodimeric variants outcompeted monovalent CD28-Fc with similar potency (Figures S7I and S7J). To directly assess binding valency, fusion proteins were incubated with *cis*-CD80:PD-L1 clone 12 cells, and then unoccupied ligand-binding domains of cell-bound fusions were detected with fluorophore-conjugated ipilimumab (anti-CTLA4; Figure S8A). As anticipated, MonoCTLA4-Ig precluded ipilimumab association (Figure S8B). *Cis*-CD80:PD-L1 cells pre-incubated with the rigid "wild type" CTLA4 homodimeric fusions abatacept and (Dim)CTLA4-Ig showed ipilimumab staining (Figure S8B), indicating that some fusion binding was monovalent. In contrast, abatacept binding to CD80-only cells was uniformly bivalent (Figure S8C). These data suggest an equilibrium where PD-L1 *cis* interactions with CD80 partially inhibit the bivalent bridging of two CD80 molecules by abatacept (Figure 6D, left), resulting in some monovalent abatacept binding. This is consistent with a previous report showing that PD-L1 overexpression can inhibit CD80:CTLA4 interactions.[35] However, abatacept at higher and therapeutically relevant concentrations released PD-L1 (Figures 1D and 6C), suggesting an equilibrium shift toward bivalent crosslinking that reorients CD80 at the expense of PD-L1 binding, consistent with previously reported split luciferase assays[40] (Figure 6D, right).

Notably, binding of FlexCTLA4-Ig variants to *cis*-CD80:PD-L1 cells precluded subsequent ipilimumab binding (Figures 6B, S8D, and S8E). This was not due to altered ipilimumab recognition because pre-incubation with ipilimumab prevented FlexCTLA4-Ig cell binding (Figure S8F). These results suggest that relaxing rigid-body CTLA4 homodimerization allows uniformly bivalent binding of FlexCTLA4-Ig to surface *cis*-CD80:PD-L1 complexes without displacing PD-L1 (Figure 6E). Consistent with this interpretation, FlexCTLA4-Ig variants were

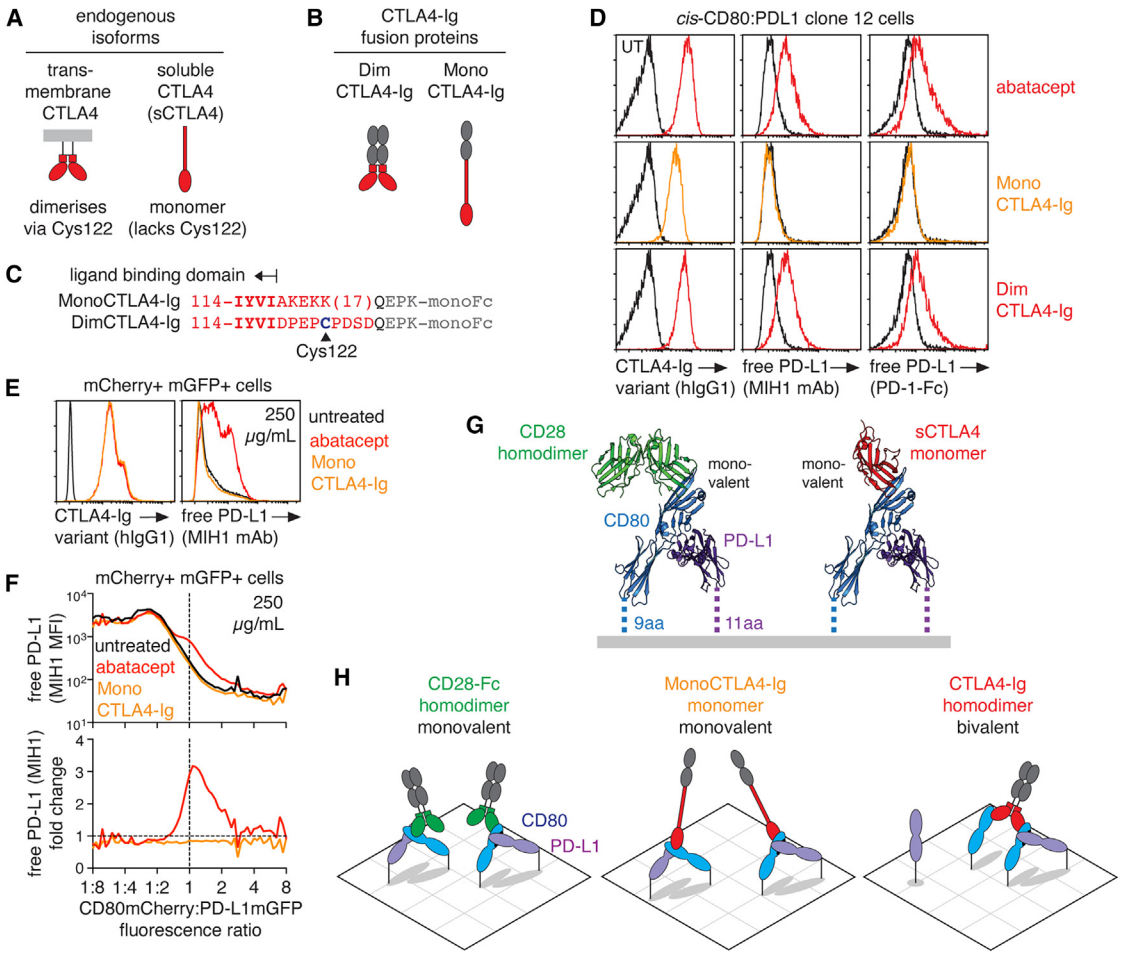

Figure 5. Monovalent sCTLA4 and CD28-Fc do not disrupt *cis*-CD80:PD-L1 duplexes

(A) Schematic of endogenous CTLA4 isoforms. Regions involved in transmembrane CTLA4 homodimerization are shown as squares, disulfide bonded through Cys122.

(B) Engineered CTLA4-Ig fusion proteins. MonoCTLA4-Ig and DimCTLA4-Ig include a human IgG1 Fc domain (gray) with S364N, Y407N, and K409T mutations that prevent dimerization (monoFc).[55]

(C) CTLA4-Ig variant protein alignment showing the C-terminal residues of the CTLA4 ligand-binding domain (bold) followed by divergent sCTLA4 and transmembrane CTLA4 sequences. Disulfide-bonded CTLA4 Cys122 is shown in blue, and residues of fused human IgG1 Fc domain are shown in gray.

(D) Flow cytometry of *cis*-CD80:PD-L1 cells incubated with CTLA4-Ig fusion proteins (red), showing fusion protein binding (hIgG1 antibody), or free PD-L1 assessed by MIH1 antibody or PD-1-Fc binding. Each stain was performed in a different tube to avoid potential MonoCTLA4-Ig crosslinking by anti-IgG1 antibodies. Gated on singlets.

(E) Flow cytometry of abatacept (red) or MonoCTLA4-Ig (orange) binding (hIgG1 staining) and resulting free PD-L1 (MIH1 staining) on CD80mCherry:PD-L1mGFP cells.

(F) Average free PD-L1 (MIH1 MFI) across CD80mCherry:PD-L1mGFP ratio intervals when untreated or treated with abatacept or MonoCTLA4-Ig (top). The same data, expressed as free PD-L1 fold change (relative to untreated) in response to abatacept and MonoCTLA4-Ig, are shown below.

(G) Structure of the human *cis*-CD80:PD-L1 duplex[39] overlaying monovalent interactions with a CD28 homodimer (left) or monomeric CTLA4 (right). Overlays are based the CTLA4:CD80 structure.[4]

(H) Models of MonoCTLA4-Ig, CD28-Fc, and CTLA4-Ig binding to *cis*-CD80:PD-L1 complexes.

immunosuppressive in T cell assays with aAPC clone 5 (Figure 4E), but unlike abatacept, their effects were not reversed by PD-1 blockade (Figure 6F).

Amelioration of inflammatory arthritis by CTLA4-Ig is nullified by PD-L1 blockade

In rheumatoid arthritis patients and mouse models of inflammatory arthritis, disease amelioration by abatacept/CTLA4-Ig is thought to be mediated by APC surface CD80 and CD86 blockade.[16–19,57] Having shown that PD-L1 liberation can contribute to T cell inhibition by CTLA4-Ig *in vitro* only when the CD80:PD-L1 ratio is below 2:1, we sought to address whether it contributes *in vivo* using a mouse model of collagen-induced arthritis (CIA), where CTLA4-Ig has proven therapeutic efficacy[57] (Figure 7A). To compare CTLA4-Ig and Flex5CTLA4-Ig *in vivo*, we generated versions with IgG1 Fc "LALA-PG"

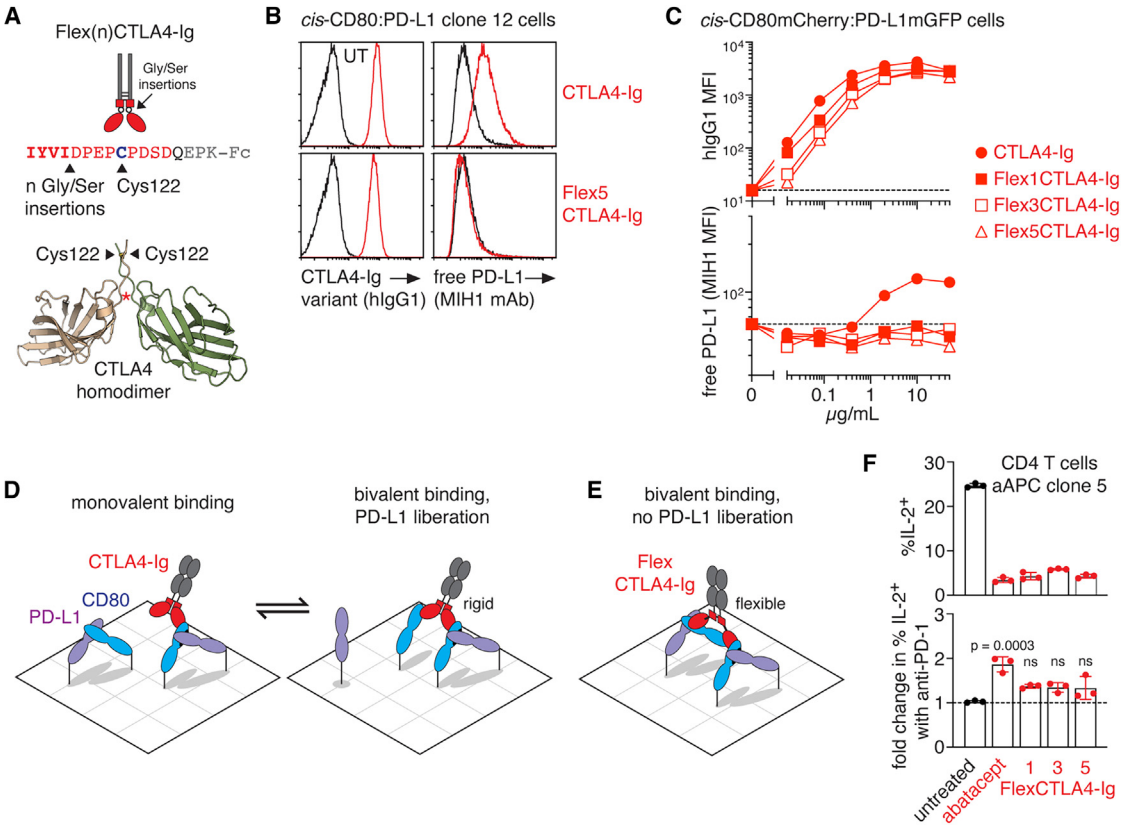

Figure 6. Flexible bivalent CTLA4-Ig variants do not liberate PD-L1 from *cis*-CD80

(A) Schematic of Flex(n)CTLA4-Ig (top), including a human IgG1 Fc domain (gray) with a C220S mutation but retaining IgG1 Cys226 and Cys229 to promote interchain disulfide bonding. The protein sequence (center) indicates the FlexCTLA4-Ig Gly/Ser insertion site, marked by a red asterisk in the CTLA4 homodimer structure (PDB: 3OSK)[2] (bottom).

(B) Flow cytometry of *cis*-CD80:PD-L1 cells as described in Figure 5D following incubation with CTLA4-Ig or Flex5CTLA4-Ig.

(C) Free PD-L1 assessed by MIH1 antibody staining (top) upon binding of CTLA4-Ig variants to CD80mCherry:PD-L1mGFP cells measured by anti-hIgG1 antibody staining (bottom).

(D) Model of monovalent abatacept binding to intact *cis*-CD80:PD-L1 complexes (left) in equilibrium with bivalent CD80 binding associated with PD-L1 liberation by a "drawbridge" mechanism (right).

(E) Model of bivalent FlexCTLA4-Ig binding two *cis*-CD80:PD-L1 complexes.

(F) Percentage of IL-2$^+$ CD4 T cells (top) treated as in Figure 4J with abatacept or FlexCTLA4-Ig variants. The corresponding fold change in the percentage of IL-2$^+$ CD4 T cells by anti-PD-1 co-treatment is shown below. Mean ± SD, n = 3, one-way ANOVA.

mutations that abrogate Fc receptor binding.[58] In the CIA mouse arthritis model, control CTLA4-Ig suppressed disease to a similar extent as clinical-grade abatacept, verifying Fc-independent activity (Figure S8G). Notably, the Flex5CTLA4-Ig fusion, which lacks PD-L1-liberating activity, failed to ameliorate arthritis but, rather, resulted in modest exacerbation of disease (Figure S8G). This was unexpected because previous studies indicate that costimulation blockade alone can alleviate CIA.[57] Upon further investigation of FlexCTLA4-Ig variants, we found that, although binding to mouse CD80 was similar to rigid CTLA4-Ig, CD86 binding was partially reduced (Figures S8H and S8I). This suggests that costimulation blockade by FlexCTLA4-Ig biologics may be compromised, making it difficult to interpret their *in vivo* effects.

As an orthogonal approach to assessing *in vivo* PD-L1/PD-1 checkpoint agonism by CTLA4-Ig, we hypothesized that PD-L1 blockade may partially reverse CTLA4-Ig anti-arthritic effects. Indeed, the clinical anti-human PD-L1 antibody atezolizumab, which also blocks mouse PD-L1, nullified the anti-inflammatory effects of abatacept in the CIA model (Figure S8J). However, in this experiment, atezolizumab monotherapy exacerbated arthritis, suggesting that coadministration of abatacept and atezolizumab may simply nullify the effects of each in this model (Figure S8J). To examine this further, we repeated the CIA experiment but also included a monovalent anti-mouse CD28 antibody that specifically blocks costimulation.[59] Tested in parallel, anti-CD28 and CTLA4-Ig each ameliorated arthritis (Figures 7B and 7C). Although disease alleviation by CD28 blockade was partially reversed by atezolizumab across the experimental time course (Figure 7C), this effect was less pronounced than for abatacept (Figure 7B). At the experimental endpoint, atezolizumab worsened the arthritis scores of vehicle-treated mice (from 8.8 to

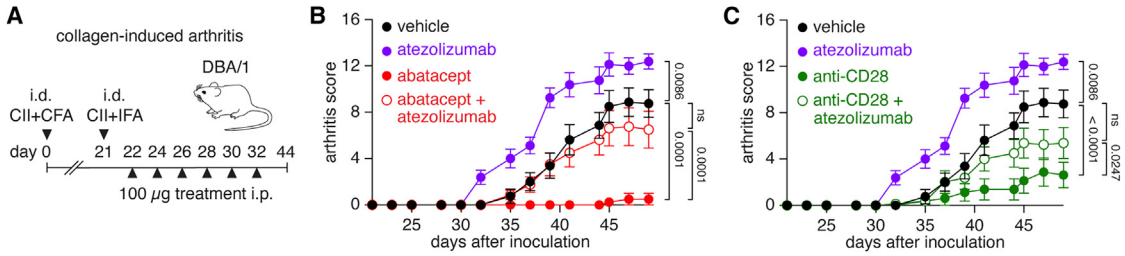

Figure 7. PD-L1 blockade nullifies CTLA4-Ig immunosuppression *in vivo*

(A) CIA model.

(B and C) Arthritis scores after treatment of CIA mice with abatacept (CTLA4-Ig) and/or atezolizumab (anti-PD-L1) (B) or PV1 (monovalent anti-mouse CD28 scFv) and/or atezolizumab (C). Mean ± SEM, n = 8 mice per group, two-way ANOVA with Tukey's multiple-comparisons test.

12.4, 1.4-fold) and anti-CD28-treated mice (from 2.6 to 5.4, 2-fold) to a similar degree (Figure 7C). In comparison, endpoint arthritis scores of abatacept-treated mice were worsened by atezolizumab to a greater extent (0.5–6.5, 13-fold), suggesting more PD-L1/PD-1 checkpoint engagement by abatacept in this context (Figure 7B). Since the PD-L1:PD-1 checkpoint clearly limits disease in this CIA model, it is possible that the cancellation of the abatacept therapeutic effect by atezolizumab results from general checkpoint blockade rather than specific blockade of PD-L1 released by abatacept. However, our *in vivo* observations are also consistent with the possibility that CTLA4-Ig may limit pathogenic inflammation by triggering the PD-L1/PD-1 checkpoint in addition to blocking costimulation.

DISCUSSION

The CTLA4-Ig therapeutics abatacept and belatacept are used widely in immune-mediated arthritis and transplant-related inflammatory disease.[17] To date, immunosuppression by CTLA4-Ig has been attributed solely to blockade of CD80/CD86 costimulation.[16,17] We show here that release of PD-L1 from *cis*-CD80:PD-L1 complexes can contribute to T cell inhibition by CTLA4-Ig but only in specific contexts. Our results do not diminish the therapeutic importance of CD80/CD86 blockade by CTLA4-Ig. Indeed, we show that CTLA4-Ig can suppress T cell activity in the absence of PD-1, in keeping with previous observations.[26] However, we also identify specific contexts where CTLA4-Ig can simultaneously block costimulation and engage the PD-L1/PD-1 checkpoint, broadening the mechanism of action of these common immunosuppressive therapies.

Our study establishes the potential of PD-1 checkpoint agonism by CTLA4-Ig therapies but also highlights two major limitations to this immune inhibitory mechanism. First, assessing many thousands of cells with different CD80:PD-L1 expression ratios demonstrates that CTLA4-Ig does not release PD-L1 from CD80 when surface CD80 expression exceeds PD-L1 by 2-fold or more. Second, even in optimal CD80:PD-L1 ratio contexts, PD-L1 release by CTLA4-Ig is well below the levels seen with PD-L1-competitive anti-CD80 antibodies. Our observations, together with previously reported structural analyses, support a PD-L1 half-liberation model where rigid CTLA4-Ig bivalently bridges one *cis*-CD80:PD-L1 complex and one free CD80 molecule. Thus, CTLA4-Ig can at best only release half of total surface PD-L1 molecules from CD80. This mechanism contrasts with PD-L1-competing anti-CD80 antibodies,[38] which can release PD-L1 in a CD80:PD-L1 ratio-independent and near-complete manner. Despite superior PD-1 agonism by these antibodies, unlike CTLA4-Ig they do not block CD80:CD28 costimulation.[38] Hence, although both classes of biologics can disrupt *cis*-CD80:PD-L1 complexes, their fundamentally different biophysical mechanisms are likely to yield distinct therapeutic activities.

The CD80:PD-L1 ratio dependence of CTLA4-Ig activity may explain previous conflicting reports as to whether CTLA4-Ig releases PD-L1.[41,42] Importantly, it also predicts that CTLA4-Ig effects will change as endogenous CD80 and PD-L1 expression varies in response to inflammatory stimuli and disease state. CD80 is upregulated by APC activation and chronic inflammation, and PD-L1 is induced by various inflammatory stimuli, including interferons.[17,32] The APC surface CD80:PD-L1 ratio also changes upon CD80 transendocytosis by CTLA4-expressing cells, which leaves free PD-L1 behind.[42] CTLA4 and PD-1 expression levels on effector T cells and Treg cells may also determine whether CTLA4-induced PD-L1 liberation regulates their activity. Since liganded PD-1 dampens both TCR and CD28 signaling,[28–31] CTLA4-induced PD-L1 liberation may differentially regulate T cell priming based on antigenic stimulus and the stage and type of autoimmune or inflammatory disease. These are important considerations when deploying CTLA4-Ig biologics as prophylactic or interventional therapies.

Our structural and functional analyses indicate that CTLA4-Ig rigidity and bivalency are both required to release PD-L1 from *cis*-CD80. Rigid homodimerization of CTLA4-Ig (and transmembrane CTLA4) occurs via a highly conserved interface involving the ligand-binding domains and adjacent regions, including an interchain disulfide bond.[2] Introducing flexibility between the two ligand-binding domains of CTLA4-Ig produces biologics that bivalently bind *cis*-CD80:PD-L1 complexes without releasing PD-L1. Hence, CTLA4-Ig indirectly triggers PD-L1 release by reorganizing cell surface CD80 into positions incompatible with PD-L1 binding. This mechanism is not engaged by CD28-Fc and transmembrane CD28 because their interactions with CD80 are monovalent.[5,6] Therefore, although CTLA4 and CD28 are both homodimers that bind CD80/CD86, their binding valency determines whether they trigger the PD-L1/PD-1 inhibitory checkpoint.

CTLA4-Ig biologics and endogenous transmembrane CTLA4 both liberate PD-L1 from *cis*-CD80.[41] Our model of PD-L1 half-liberation by CTLA4-Ig involves tilting of CD80-bound CTLA4-Ig oblique to the APC cell surface. In the context of CTLA4-expressing T cell interactions with *cis*-CD80:PD-L1-expressing APCs, such re-orientation of transmembrane CTLA4 may by impeded by CTLA4 membrane anchoring and/or synaptic CD80:CTLA4 crosslinking.[4,60] Indeed, membrane-perpendicular CTLA4:CD80 binding (potentially followed by CD80 transendocytosis or trogocytosis) is predicted to trigger PD-L1 full liberation on the APC surface, allowing PD-1 engagement on synapsed T cells.[41,42] This may occur when CTLA4-replete Treg cells interact with dendritic cells, which can express abundant *cis*-CD80:PD-L1 complexes.[34] Regardless of the exact mechanism, Treg cell surface CTLA4 is predicted to render dendritic cells potently tolerogenic by simultaneously blocking CD80/CD86 and releasing PD-L1. In contrast to other PD-L1-regulatory mechanisms,[32] CTLA4-induced liberation immediately engages PD-L1-inhibitory functions without altering its expression.

Our observations are also relevant to therapeutic CTLA4 and PD-(L)1 checkpoint blockade in cancer. If APCs express surface CD80 and PD-L1, then CTLA4 blockade (e.g., with ipilimumab) or Treg cell depletion should allow CD80 to sequester PD-L1. In this scenario, CTLA4 inhibition is predicted to trigger CD28 costimulatory signaling while simultaneously protecting it (and TCR signaling) from PD-1 inhibition. This CD80-dependent mechanism is notable, given recent reports that PD-L1 expressed on dendritic cells, rather than tumor cells, suppresses antitumor immunity.[36,37,61,62] Our work contributes further understanding of how CTLA4-induced PD-L1 liberation regulates T cell immunity in different biological contexts, which may improve the rational use of checkpoint agonists or inhibitors in autoimmunity and cancer.

Limitations of the study

As indicated earlier, the mouse data here do not conclusively demonstrate a functional role for PD-L1 release in immunosuppression by CTLA4-Ig *in vivo*. Having demonstrated that CTLA4-Ig therapies can engage the PD-L1 checkpoint only at defined CD80:PD-L1 ratios, it remains to be seen where and when this context arises *in vivo*. This may be determined through further study of mouse and human autoimmune and inflammatory diseases.

RESOURCE AVAILABILITY

Lead contact

Requests for further information and resources should be directed to and will be fulfilled by the lead contact, Ross Dickins (ross.dickins@monash.edu).

Materials availability

Reagents generated in this study will be made available upon request but may require a materials transfer agreement if there is potential for commercial application.

Data and code availability

- Data may be made available upon request by the lead contact.
- This paper does not report original code.
- Any additional information required to reanalyze the data reported in this paper is available from the lead contact upon request.

ACKNOWLEDGMENTS

We thank Tania Camilleri, Sandra Esparon, Bruce Wines, Volga Tarlac, Huon Wong, and the Alfred Research Alliance Flow Cytometry Core Facility for experimental assistance and Mark Shackleton, Grant McArthur, John Coutsevoulis, Bianca Tong, Jonathan Akikusa, and Antun Bogovic for reagents. We thank Tanya Puhalovich and Marija Dramicanin at the WEHI Protein Production Facility for assistance with endotoxin-free protein production and SEC-MALS. We thank Justin Hamilton, Jeff Babon, Peter Czabotar, John Hamilton, Alex Barrow, and Accelerating Cancer Immunotherapy Research (ACIR) for insights. M.C.v.Z. is supported by Australian National Health and Medical Research Council (NHMRC) Senior Research Fellowship 1117687. N.M.H. is supported by the imCORE Network on behalf of F. Hoffmann-La Roche Ltd. and the II-ON network on behalf of Bristol Myers Squibb. I.P.W. is supported by NHMRC Program Grant 1023407 and Clinical Practitioner Fellowship 1154325, the Reid Charitable Trusts, Victorian State Government Operational Infrastructure Support, and the NHMRC Independent Research Institute Infrastructure Support scheme. N.D.H. is supported by NHMRC Project Grant 115995, Ideas Grant 118461, and Investigator Fellowship 119529. R.A.D. is supported by a CUREator grant from the Australian Government Medical Research Future Fund.

AUTHOR CONTRIBUTIONS

E.P.O., N.J.K., C.L., K.J.G., M.M.G., M.C.v.Z., M.O., P.M.H., N.M.H., N.D.H., I.P.W., and R.A.D. designed experiments. E.P.O., N.J.K., C.L., K.J.G., M.M.G., S.M.J.H., H.-Y.P., J.I., L.L.L.W., A.G.L., S.W., E.S.J.E., D.B.D., J.H., E.S.P., V.T.F.V., and N.M.H. performed experiments and analyzed data. R.A.D. conceived the study and wrote the paper with input from authors.

DECLARATION OF INTERESTS

E.P.O., N.J.K., K.J.G., M.M.G., and R.A.D. are inventors on International Patent Application PCT/AU2022/051296 (filed October 28, 2022) related to this work. E.P.O., N.J.K., and R.A.D. are co-founders of FLEX Immunotherapeutics. N.D.H. is CSO of oNKo-Innate Pty Ltd and declares ownership and funding not related to this work.

STAR★METHODS

Detailed methods are provided in the online version of this paper and include the following:

- KEY RESOURCES TABLE
- EXPERIMENTAL MODEL AND STUDY PARTICIPANT DETAILS
- METHOD DETAILS
  - Surface protein vector cloning
  - Fluorescent fusion protein vector cloning
  - Recombinant antibody and Ig fusion protein vector cloning
  - Protein expression and purification
  - Size-exclusion chromatography – Multi-angle light scattering (SEC-MALS)
  - Commercial recombinant Fc fusion proteins
  - Cell culture
  - Cell-cell interaction assays
  - RAW264.7 cell knockdown
  - Flow cytometry of cultured cells
  - CD80mCherry:PD-L1mGFP population analysis
  - Cell dissociation assay
  - Primary human T cell assays
  - Collagen induced arthritis (CIA) mouse model
- QUANTIFICATION AND STATISTICAL ANALYSIS

SUPPLEMENTAL INFORMATION

Supplemental information can be found online at https://doi.org/10.1016/j.celrep.2024.114834.

Received: June 1, 2023
Revised: August 30, 2024
Accepted: September 19, 2024
Published: October 8, 2024

REFERENCES

1. Rowshanravan, B., Halliday, N., and Sansom, D.M. (2018). CTLA-4: a moving target in immunotherapy. Blood *131*, 58–67. https://doi.org/10.1182/blood-2017-06-741033.
2. Yu, C., Sonnen, A.F.P., George, R., Dessailly, B.H., Stagg, L.J., Evans, E.J., Orengo, C.A., Stuart, D.I., Ladbury, J.E., Ikemizu, S., et al. (2011). Rigid-body ligand recognition drives cytotoxic T-lymphocyte antigen 4 (CTLA-4) receptor triggering. J. Biol. Chem. *286*, 6685–6696. https://doi.org/10.1074/jbc.M110.182394.
3. Linsley, P.S., Nadler, S.G., Bajorath, J., Peach, R., Leung, H.T., Rogers, J., Bradshaw, J., Stebbins, M., Leytze, G., and Brady, W. (1995). Binding stoichiometry of the cytotoxic T lymphocyte-associated molecule-4 (CTLA-4). A disulfide-linked homodimer binds two CD86 molecules. J. Biol. Chem. *270*, 15417–15424. https://doi.org/10.1074/jbc.270.25.15417.
4. Stamper, C.C., Zhang, Y., Tobin, J.F., Erbe, D.V., Ikemizu, S., Davis, S.J., Stahl, M.L., Seehra, J., Somers, W.S., and Mosyak, L. (2001). Crystal structure of the B7-1/CTLA-4 complex that inhibits human immune responses. Nature *410*, 608–611. https://doi.org/10.1038/35069118.
5. Collins, A.V., Brodie, D.W., Gilbert, R.J.C., Iaboni, A., Manso-Sancho, R., Walse, B., Stuart, D.I., van der Merwe, P.A., and Davis, S.J. (2002). The interaction properties of costimulatory molecules revisited. Immunity *17*, 201–210. https://doi.org/10.1016/s1074-7613(02)00362-x.
6. Evans, E.J., Esnouf, R.M., Manso-Sancho, R., Gilbert, R.J.C., James, J.R., Yu, C., Fennelly, J.A., Vowles, C., Hanke, T., Walse, B., et al. (2005). Crystal structure of a soluble CD28-Fab complex. Nat. Immunol. *6*, 271–279. https://doi.org/10.1038/ni1170.
7. Wing, K., Onishi, Y., Prieto-Martin, P., Yamaguchi, T., Miyara, M., Fehervari, Z., Nomura, T., and Sakaguchi, S. (2008). CTLA-4 control over Foxp3+ regulatory T cell function. Science *322*, 271–275. https://doi.org/10.1126/science.1160062.
8. Qureshi, O.S., Zheng, Y., Nakamura, K., Attridge, K., Manzotti, C., Schmidt, E.M., Baker, J., Jeffery, L.E., Kaur, S., Briggs, Z., et al. (2011). Trans-endocytosis of CD80 and CD86: a molecular basis for the cell-extrinsic function of CTLA-4. Science *332*, 600–603. https://doi.org/10.1126/science.1202947.
9. Kuehn, H.S., Ouyang, W., Lo, B., Deenick, E.K., Niemela, J.E., Avery, D.T., Schickel, J.N., Tran, D.Q., Stoddard, J., Zhang, Y., et al. (2014). Immune dysregulation in human subjects with heterozygous germline mutations in CTLA4. Science *345*, 1623–1627. https://doi.org/10.1126/science.1255904.
10. Schubert, D., Bode, C., Kenefeck, R., Hou, T.Z., Wing, J.B., Kennedy, A., Bulashevska, A., Petersen, B.S., Schäffer, A.A., Grüning, B.A., et al. (2014). Autosomal dominant immune dysregulation syndrome in humans with CTLA4 mutations. Nat. Med. *20*, 1410–1416. https://doi.org/10.1038/nm.3746.
11. Tivol, E.A., Borriello, F., Schweitzer, A.N., Lynch, W.P., Bluestone, J.A., and Sharpe, A.H. (1995). Loss of CTLA-4 leads to massive lymphoproliferation and fatal multiorgan tissue destruction, revealing a critical negative regulatory role of CTLA-4. Immunity *3*, 541–547.
12. Waterhouse, P., Penninger, J.M., Timms, E., Wakeham, A., Shahinian, A., Lee, K.P., Thompson, C.B., Griesser, H., and Mak, T.W. (1995). Lymphoproliferative disorders with early lethality in mice deficient in Ctla-4. Science *270*, 985–988.
13. Wei, S.C., Duffy, C.R., and Allison, J.P. (2018). Fundamental Mechanisms of Immune Checkpoint Blockade Therapy. Cancer Discov. *8*, 1069–1086. https://doi.org/10.1158/2159-8290.CD-18-0367.
14. Ramos-Casals, M., Brahmer, J.R., Callahan, M.K., Flores-Chávez, A., Keegan, N., Khamashta, M.A., Lambotte, O., Mariette, X., Prat, A., and Suárez-Almazor, M.E. (2020). Immune-related adverse events of checkpoint inhibitors. Nat. Rev. Dis. Prim. *6*, 38. https://doi.org/10.1038/s41572-020-0160-6.
15. Linsley, P.S., Brady, W., Urnes, M., Grosmaire, L.S., Damle, N.K., and Ledbetter, J.A. (1991). CTLA-4 is a second receptor for the B cell activation antigen B7. J. Exp. Med. *174*, 561–569.
16. Bonelli, M., and Scheinecker, C. (2018). How does abatacept really work in rheumatoid arthritis? Curr. Opin. Rheumatol. *30*, 295–300. https://doi.org/10.1097/BOR.0000000000000491.
17. Edner, N.M., Carlesso, G., Rush, J.S., and Walker, L.S.K. (2020). Targeting co-stimulatory molecules in autoimmune disease. Nat. Rev. Drug Discov. *19*, 860–883. https://doi.org/10.1038/s41573-020-0081-9.
18. Kremer, J.M., Westhovens, R., Leon, M., Di Giorgio, E., Alten, R., Steinfeld, S., Russell, A., Dougados, M., Emery, P., Nuamah, I.F., et al. (2003). Treatment of rheumatoid arthritis by selective inhibition of T-cell activation with fusion protein CTLA4Ig. N. Engl. J. Med. *349*, 1907–1915. https://doi.org/10.1056/NEJMoa035075.
19. Genovese, M.C., Becker, J.C., Schiff, M., Luggen, M., Sherrer, Y., Kremer, J., Birbara, C., Box, J., Natarajan, K., Nuamah, I., et al. (2005). Abatacept for rheumatoid arthritis refractory to tumor necrosis factor alpha inhibition. N. Engl. J. Med. *353*, 1114–1123. https://doi.org/10.1056/NEJMoa050524.
20. Larsen, C.P., Pearson, T.C., Adams, A.B., Tso, P., Shirasugi, N., Strobert, E., Anderson, D., Cowan, S., Price, K., Naemura, J., et al. (2005). Rational development of LEA29Y (belatacept), a high-affinity variant of CTLA4-Ig with potent immunosuppressive properties. Am. J. Transplant. *5*, 443–453. https://doi.org/10.1111/j.1600-6143.2005.00749.x.
21. Vincenti, F., Rostaing, L., Grinyo, J., Rice, K., Steinberg, S., Gaite, L., Moal, M.C., Mondragon-Ramirez, G.A., Kothari, J., Polinsky, M.S., et al. (2016). Belatacept and Long-Term Outcomes in Kidney Transplantation. N. Engl. J. Med. *374*, 333–343. https://doi.org/10.1056/NEJMoa1506027.
22. Watkins, B., Qayed, M., McCracken, C., Bratrude, B., Betz, K., Suessmuth, Y., Yu, A., Sinclair, S., Furlan, S., Bosinger, S., et al. (2021). Phase II Trial of Costimulation Blockade With Abatacept for Prevention of Acute GVHD. J. Clin. Oncol. *39*, 1865–1877. https://doi.org/10.1200/JCO.20.01086.
23. Cope, A.P., Jasenecova, M., Vasconcelos, J.C., Filer, A., Raza, K., Qureshi, S., D'Agostino, M.A., McInnes, I.B., Isaacs, J.D., Pratt, A.G., et al. (2024). Abatacept in individuals at high risk of rheumatoid arthritis (APIPPRA): a randomised, double-blind, multicentre, parallel, placebo-controlled, phase 2b clinical trial. Lancet *403*, 838–849. https://doi.org/10.1016/S0140-6736(23)02649-1.
24. Rech, J., Tascilar, K., Hagen, M., Kleyer, A., Manger, B., Schoenau, V., Hueber, A.J., Kleinert, S., Baraliakos, X., Braun, J., et al. (2024). Abatacept inhibits inflammation and onset of rheumatoid arthritis in individuals at high risk (ARIAA): a randomised, international, multicentre, double-blind, placebo-controlled trial. Lancet *403*, 850–859. https://doi.org/10.1016/S0140-6736(23)02650-8.
25. Salem, J.E., Allenbach, Y., Vozy, A., Brechot, N., Johnson, D.B., Moslehi, J.J., and Kerneis, M. (2019). Abatacept for Severe Immune Checkpoint Inhibitor-Associated Myocarditis. N. Engl. J. Med. *380*, 2377–2379. https://doi.org/10.1056/NEJMc1901677.
26. Wei, S.C., Meijers, W.C., Axelrod, M.L., Anang, N.A.A.S., Screever, E.M., Wescott, E.C., Johnson, D.B., Whitley, E., Lehmann, L., Courand, P.Y., et al. (2021). A genetic mouse model recapitulates immune checkpoint inhibitor-associated myocarditis and supports a mechanism-based therapeutic intervention. Cancer Discov. *11*, 614–625. https://doi.org/10.1158/2159-8290.CD-20-0856.
27. Salem, J.E., Bretagne, M., Abbar, B., Leonard-Louis, S., Ederhy, S., Redheuil, A., Boussouar, S., Nguyen, L.S., Procureur, A., Stein, F., et al. (2023). Abatacept/Ruxolitinib and Screening for Concomitant Respiratory Muscle Failure to Mitigate Fatality of Immune-Checkpoint Inhibitor Myocarditis. Cancer Discov. *13*, 1100–1115. https://doi.org/10.1158/2159-8290.CD-22-1180.

28. Hui, E., Cheung, J., Zhu, J., Su, X., Taylor, M.J., Wallweber, H.A., Sasmal, D.K., Huang, J., Kim, J.M., Mellman, I., and Vale, R.D. (2017). T cell costimulatory receptor CD28 is a primary target for PD-1-mediated inhibition. Science *355*, 1428–1433. https://doi.org/10.1126/science.aaf1292.

29. Kamphorst, A.O., Wieland, A., Nasti, T., Yang, S., Zhang, R., Barber, D.L., Konieczny, B.T., Daugherty, C.Z., Koenig, L., Yu, K., et al. (2017). Rescue of exhausted CD8 T cells by PD-1-targeted therapies is CD28-dependent. Science *355*, 1423–1427. https://doi.org/10.1126/science.aaf0683.

30. Mizuno, R., Sugiura, D., Shimizu, K., Maruhashi, T., Watada, M., Okazaki, I.M., and Okazaki, T. (2019). PD-1 Primarily Targets TCR Signal in the Inhibition of Functional T Cell Activation. Front. Immunol. *10*, 630. https://doi.org/10.3389/fimmu.2019.00630.

31. Elliot, T.A.E., Jennings, E.K., Lecky, D.A.J., Thawait, N., Flores-Langarica, A., Copland, A., Maslowski, K.M., Wraith, D.C., and Bending, D. (2021). Antigen and checkpoint receptor engagement recalibrates T cell receptor signal strength. Immunity *54*, 2481–2496.e6. https://doi.org/10.1016/j.immuni.2021.08.020.

32. Sun, C., Mezzadra, R., and Schumacher, T.N. (2018). Regulation and Function of the PD-L1 Checkpoint. Immunity *48*, 434–452. https://doi.org/10.1016/j.immuni.2018.03.014.

33. Chaudhri, A., Xiao, Y., Klee, A.N., Wang, X., Zhu, B., and Freeman, G.J. (2018). PD-L1 Binds to B7-1 Only In Cis on the Same Cell Surface. Cancer Immunol. Res. *6*, 921–929. https://doi.org/10.1158/2326-6066.CIR-17-0316.

34. Sugiura, D., Maruhashi, T., Okazaki, I.M., Shimizu, K., Maeda, T.K., Takemoto, T., and Okazaki, T. (2019). Restriction of PD-1 function by cis-PD-L1/CD80 interactions is required for optimal T cell responses. Science *364*, 558–566. https://doi.org/10.1126/science.aav7062.

35. Zhao, Y., Lee, C.K., Lin, C.H., Gassen, R.B., Xu, X., Huang, Z., Xiao, C., Bonorino, C., Lu, L.F., Bui, J.D., and Hui, E. (2019). PD-L1:CD80 Cis-Heterodimer Triggers the Co-stimulatory Receptor CD28 While Repressing the Inhibitory PD-1 and CTLA-4 Pathways. Immunity *51*, 1059–1073.e9. https://doi.org/10.1016/j.immuni.2019.11.003.

36. Mayoux, M., Roller, A., Pulko, V., Sammicheli, S., Chen, S., Sum, E., Jost, C., Fransen, M.F., Buser, R.B., Kowanetz, M., et al. (2020). Dendritic cells dictate responses to PD-L1 blockade cancer immunotherapy. Sci. Transl. Med. *12*, eaav7431. https://doi.org/10.1126/scitranslmed.aav7431.

37. Oh, S.A., Wu, D.C., Cheung, J., Navarro, A., Xiong, H., Cubas, R., Totpal, K., Chiu, H., Wu, Y., Comps-Agrar, L., et al. (2020). PD-L1 expression by dendritic cells is a key regulator of T-cell immunity in cancer. Nat. Can. (Ott.) *1*, 681–691. https://doi.org/10.1038/s43018-020-0075-x.

38. Sugiura, D., Okazaki, I.M., Maeda, T.K., Maruhashi, T., Shimizu, K., Arakaki, R., Takemoto, T., Ishimaru, N., and Okazaki, T. (2022). PD-1 agonism by anti-CD80 inhibits T cell activation and alleviates autoimmunity. Nat. Immunol. *23*, 399–410. https://doi.org/10.1038/s41590-021-01125-7.

39. Maurer, M.F., Lewis, K.E., Kuijper, J.L., Ardourel, D., Gudgeon, C.J., Chandrasekaran, S., Mudri, S.L., Kleist, K.N., Navas, C., Wolfson, M.F., et al. (2022). The engineered CD80 variant fusion therapeutic davoceticept combines checkpoint antagonism with conditional CD28 costimulation for anti-tumor immunity. Nat. Commun. *13*, 1790. https://doi.org/10.1038/s41467-022-29286-5.

40. Garrett-Thomson, S.C., Massimi, A., Fedorov, E.V., Bonanno, J.B., Scandiuzzi, L., Hillerich, B., Seidel, R.D., 3rd, Love, J.D., Garforth, S.J., Guha, C., and Almo, S.C. (2020). Mechanistic dissection of the PD-L1:B7-1 co-inhibitory immune complex. PLoS One *15*, e0233578. https://doi.org/10.1371/journal.pone.0233578.

41. Tekguc, M., Wing, J.B., Osaki, M., Long, J., and Sakaguchi, S. (2021). Treg-expressed CTLA-4 depletes CD80/CD86 by trogocytosis, releasing free PD-L1 on antigen-presenting cells. Proc. Natl. Acad. Sci. USA *118*, e2023739118. https://doi.org/10.1073/pnas.2023739118.

42. Kennedy, A., Robinson, M.A., Hinze, C., Waters, E., Williams, C., Halliday, N., Dovedi, S., and Sansom, D.M. (2023). The CTLA-4 immune checkpoint protein regulates PD-L1:PD-1 interaction via transendocytosis of its ligand CD80. EMBO J. *42*, e111556. https://doi.org/10.15252/embj.2022111556.

43. Pulanco, M.C., Madsen, A.T., Tanwar, A., Corrigan, D.T., and Zang, X. (2023). Recent advancements in the B7/CD28 immune checkpoint families: new biology and clinical therapeutic strategies. Cell. Mol. Immunol. *20*, 694–713. https://doi.org/10.1038/s41423-023-01019-8.

44. Haile, S.T., Bosch, J.J., Agu, N.I., Zeender, A.M., Somasundaram, P., Srivastava, M.K., Britting, S., Wolf, J.B., Ksander, B.R., and Ostrand-Rosenberg, S. (2011). Tumor cell programmed death ligand 1-mediated T cell suppression is overcome by coexpression of CD80. J. Immunol. *186*, 6822–6829. https://doi.org/10.4049/jimmunol.1003682.

45. Butte, M.J., Peña-Cruz, V., Kim, M.J., Freeman, G.J., and Sharpe, A.H. (2008). Interaction of human PD-L1 and B7-1. Mol. Immunol. *45*, 3567–3572. https://doi.org/10.1016/j.molimm.2008.05.014.

46. Haile, S.T., Dalal, S.P., Clements, V., Tamada, K., and Ostrand-Rosenberg, S. (2013). Soluble CD80 restores T cell activation and overcomes tumor cell programmed death ligand 1-mediated immune suppression. J. Immunol. *191*, 2829–2836. https://doi.org/10.4049/jimmunol.1202777.

47. Li, X., Roy, A., and Murthy, B. (2019). Population Pharmacokinetics and Exposure-Response Relationship of Intravenous and Subcutaneous Abatacept in Patients With Rheumatoid Arthritis. J. Clin. Pharmacol. *59*, 245–257. https://doi.org/10.1002/jcph.1308.

48. Lin, D.Y.W., Tanaka, Y., Iwasaki, M., Gittis, A.G., Su, H.P., Mikami, B., Okazaki, T., Honjo, T., Minato, N., and Garboczi, D.N. (2008). The PD-1/PD-L1 complex resembles the antigen-binding Fv domains of antibodies and T cell receptors. Proc. Natl. Acad. Sci. USA *105*, 3011–3016. https://doi.org/10.1073/pnas.0712278105.

49. Zak, K.M., Kitel, R., Przetocka, S., Golik, P., Guzik, K., Musielak, B., Dömling, A., Dubin, G., and Holak, T.A. (2015). Structure of the Complex of Human Programmed Death 1, PD-1, and Its Ligand PD-L1. Structure *23*, 2341–2348. https://doi.org/10.1016/j.str.2015.09.010.

50. Lee, H.T., Lee, J.Y., Lim, H., Lee, S.H., Moon, Y.J., Pyo, H.J., Ryu, S.E., Shin, W., and Heo, Y.S. (2017). Molecular mechanism of PD-1/PD-L1 blockade via anti-PD-L1 antibodies atezolizumab and durvalumab. Sci. Rep. *7*, 5532. https://doi.org/10.1038/s41598-017-06002-8.

51. Douthwaite, J., Moisan, J., Privezentzev, C., Soskic, B., Sabbah, S., Cohen, S., Collinson, A., England, E., Huntington, C., Kemp, B., et al. (2017). A CD80-Biased CTLA4-Ig Fusion Protein with Superior In Vivo Efficacy by Simultaneous Engineering of Affinity, Selectivity, Stability, and FcRn Binding. J. Immunol. *198*, 528–537. https://doi.org/10.4049/jimmunol.1600682.

52. Shimizu, K., Sugiura, D., Okazaki, I.M., Maruhashi, T., Takegami, Y., Cheng, C., Ozaki, S., and Okazaki, T. (2020). PD-1 Imposes Qualitative Control of Cellular Transcriptomes in Response to T Cell Activation. Mol. Cell *77*, 937–950.e6. https://doi.org/10.1016/j.molcel.2019.12.012.

53. Suchard, S.J., Davis, P.M., Kansal, S., Stetsko, D.K., Brosius, R., Tamura, J., Schneeweis, L., Bryson, J., Salcedo, T., Wang, H., et al. (2013). A monovalent anti-human CD28 domain antibody antagonist: preclinical efficacy and safety. J. Immunol. *191*, 4599–4610. https://doi.org/10.4049/jimmunol.1300470.

54. Dahal, L.N., Schwarz, H., and Ward, F.J. (2018). Hiding in Plain Sight: Soluble Immunomodulatory Receptors. Trends Immunol. *39*, 771–774. https://doi.org/10.1016/j.it.2018.08.004.

55. Ishino, T., Wang, M., Mosyak, L., Tam, A., Duan, W., Svenson, K., Joyce, A., O'Hara, D.M., Lin, L., Somers, W.S., and Kriz, R. (2013). Engineering a monomeric Fc domain modality by N-glycosylation for the half-life extension of biotherapeutics. J. Biol. Chem. *288*, 16529–16537. https://doi.org/10.1074/jbc.M113.457689.

56. Darlington, P.J., Kirchhof, M.G., Criado, G., Sondhi, J., and Madrenas, J. (2005). Hierarchical regulation of CTLA-4 dimer-based lattice formation and its biological relevance for T cell inactivation. J. Immunol. *175*, 996–1004. https://doi.org/10.4049/jimmunol.175.2.996.

57. Webb, L.M., Walmsley, M.J., and Feldmann, M. (1996). Prevention and amelioration of collagen-induced arthritis by blockade of the CD28 co-stimulatory pathway: requirement for both B7-1 and B7-2. Eur. J. Immunol. *26*, 2320–2328. https://doi.org/10.1002/eji.1830261008.

58. Lo, M., Kim, H.S., Tong, R.K., Bainbridge, T.W., Vernes, J.M., Zhang, Y., Lin, Y.L., Chung, S., Dennis, M.S., Zuchero, Y.J.Y., et al. (2017). Effector-attenuating Substitutions That Maintain Antibody Stability and Reduce Toxicity in Mice. J. Biol. Chem. *292*, 3900–3908. https://doi.org/10.1074/jbc.M116.767749.

59. Zhang, T., Fresnay, S., Welty, E., Sangrampurkar, N., Rybak, E., Zhou, H., Cheng, X.F., Feng, Q., Avon, C., Laaris, A., et al. (2011). Selective CD28 blockade attenuates acute and chronic rejection of murine cardiac allografts in a CTLA-4-dependent manner. Am. J. Transplant. *11*, 1599–1609. https://doi.org/10.1111/j.1600-6143.2011.03624.x.

60. Pentcheva-Hoang, T., Egen, J.G., Wojnoonski, K., and Allison, J.P. (2004). B7-1 and B7-2 selectively recruit CTLA-4 and CD28 to the immunological synapse. Immunity *21*, 401–413. https://doi.org/10.1016/j.immuni.2004.06.017.

61. Dammeijer, F., van Gulijk, M., Mulder, E.E., Lukkes, M., Klaase, L., van den Bosch, T., van Nimwegen, M., Lau, S.P., Latupeirissa, K., Schetters, S., et al. (2020). The PD-1/PD-L1-Checkpoint Restrains T cell Immunity in Tumor-Draining Lymph Nodes. Cancer Cell *38*, 685–700.e8. https://doi.org/10.1016/j.ccell.2020.09.001.

62. Peng, Q., Qiu, X., Zhang, Z., Zhang, S., Zhang, Y., Liang, Y., Guo, J., Peng, H., Chen, M., Fu, Y.X., and Tang, H. (2020). PD-L1 on dendritic cells attenuates T cell activation and regulates response to immune checkpoint blockade. Nat. Commun. *11*, 4835. https://doi.org/10.1038/s41467-020-18570-x.

63. Puck, T.T., and Fisher, H.W. (1956). GENETICS OF SOMATIC MAMMALIAN CELLS : I. DEMONSTRATION OF THE EXISTENCE OF MUTANTS WITH DIFFERENT GROWTH REQUIREMENTS IN A HUMAN CANCER CELL STRAIN (HELA). J Exp Med. *104*, 427–434.

64. Raschke, W.C., Baird, S., Ralph, P., and Nakoinz, I. (1978). Functional macrophage cell lines transformed by Abelson leukemia virus. Cell *15*, 261–267.

65. Fellmann, C., Hoffmann, T., Sridhar, V., Hopfgartner, B., Muhar, M., Roth, M., Lai, D.Y., Barbosa, I.A.M., Kwon, J.S., Guan, Y., et al. (2013). An optimized microRNA backbone for effective single-copy RNAi. Cell Rep. *5*, 1704–1713. https://doi.org/10.1016/j.celrep.2013.11.020.

66. Leitner, J., Kuschei, W., Grabmeier-Pfistershammer, K., Woitek, R., Kriehuber, E., Majdic, O., Zlabinger, G., Pickl, W.F., and Steinberger, P. (2010). T cell stimulator cells, an efficient and versatile cellular system to assess the role of costimulatory ligands in the activation of human T cells. J. Immunol. Methods *362*, 131–141. https://doi.org/10.1016/j.jim.2010.09.020.

67. Jutz, S., Hennig, A., Paster, W., Asrak, Ö., Dijanovic, D., Kellner, F., Pickl, W.F., Huppa, J.B., Leitner, J., and Steinberger, P. (2017). A cellular platform for the evaluation of immune checkpoint molecules. Oncotarget *8*, 64892–64906. https://doi.org/10.18632/oncotarget.17615.

68. Shaner, N.C., Campbell, R.E., Steinbach, P.A., Giepmans, B.N.G., Palmer, A.E., and Tsien, R.Y. (2004). Improved monomeric red, orange and yellow fluorescent proteins derived from Discosoma sp. red fluorescent protein. Nat. Biotechnol. *22*, 1567–1572. https://doi.org/10.1038/nbt1037.

69. Zacharias, D.A., Violin, J.D., Newton, A.C., and Tsien, R.Y. (2002). Partitioning of lipid-modified monomeric GFPs into membrane microdomains of live cells. Science *296*, 913–916. https://doi.org/10.1126/science.1068539.

70. Edelman, G.M., Cunningham, B.A., Gall, W.E., Gottlieb, P.D., Rutishauser, U., and Waxdal, M.J. (1969). The covalent structure of an entire gammaG immunoglobulin molecule. Proc. Natl. Acad. Sci. USA *63*, 78–85. https://doi.org/10.1073/pnas.63.1.78.

71. Ying, T., Chen, W., Gong, R., Feng, Y., and Dimitrov, D.S. (2012). Soluble monomeric IgG1 Fc. J. Biol. Chem. *287*, 19399–19408. https://doi.org/10.1074/jbc.M112.368647.

72. Louis, C., Ngo, D., D'Silva, D.B., Hansen, J., Phillipson, L., Jousset, H., Novello, P., Segal, D., Lawlor, K.E., Burns, C.J., and Wicks, I.P. (2019). Therapeutic Effects of a TANK-Binding Kinase 1 Inhibitor in Germinal Center-Driven Collagen-Induced Arthritis. Arthritis Rheumatol. *71*, 50–62. https://doi.org/10.1002/art.40670.

STAR★METHODS

KEY RESOURCES TABLE

REAGENT or RESOURCE	SOURCE	IDENTIFIER
Antibodies		
PD-L1-PE (clone MIH1)	Thermo Fisher	Cat#12-5983-42; RRID:AB_11042286
CD80-BV711 (clone L307.4)	BD Biosciences	Cat#568227; RRID:AB_2916855
PD-L1-BV605 (clone MIH6)	BioLegend	Cat#153606; RRID:AB_2814056
PD-L1-AF647 (clone MIH6)	Bio-Rad	Discontinued
PD-L1-PE-Cy7 (clone MIH5)	Thermo Fisher	Cat#25-5982-82; RRID:AB_2573509
CD80-APC (clone 16-10A1)	Thermo Fisher	Cat#17-0801-82; RRID:AB_469417
Human IgG1-APC (clone IS11-12E4.23.20)	Miltenyi Biotec	Cat#130-119-859; RRID:AB_2784378
Mouse IgG1-APC (clone RMG1-1)	BioLegend	Cat#406610; RRID:AB_10696420
Mouse IgG2a-PE-Cy7 (clone m2a-15F8)	Thermo Fisher	Cat#25-4210-82; RRID:AB_2573448
I-A/I-E MHCII-PE (clone M5/114.15.2)	BioLegend	Cat#107608; RRID:AB_313323
CD11b-BV711 (clone M1/70)	BioLegend	Cat#101242; RRID:AB_2563310
CD11c-FITC (clone HL3)	BD Biosciences	Cat#553801; RRID:AB_395060
CD8a-BV421 (clone 53–6.7)	BioLegend	Cat#100737; RRID:AB_10897101
CD28-PerCP-Cy5.5 (clone CD28.2)	BioLegend	Cat#302922; RRID:AB_2073718
CD4-BV711 (clone SK3)	BioLegend	Cat#344648; RRID:AB_2734350
IL-2-PE (clone MQ1-17H12)	BioLegend	Cat#500307; RRID:AB_315094
PD-1-CF488A (nivolumab)	Self-made	N/A
CTLA4-CF647 (ipilimumab)	Self-made	N/A
TKMG48	Self-made	N/A
TKMF5	Self-made	N/A
OPDIVO (nivolumab)	Bristol Myers Squibb	N/A
YERVOY (ipilimumab)	Bristol Myers Squibb	N/A
Tecentriq (atezolizumab)	Roche	N/A
Bacterial and virus strains		
NEB 5-alpha Competent E. coli (High Efficiency)	New England Biolabs	Cat#C2987H
Biological samples		
Healthy volunteer PBMC	ACBD, Monash University	N/A
Chemicals, peptides, and recombinant proteins		
Lipopolysaccharide	New England Biolabs	Cat#518653
Orencia (abatacept)	Bristol Myers Squibb	N/A
CTLA4-Ig	Self-made	N/A
FlexCTLA4-Ig variants	Self-made	N/A
$CTLA4^{HA}$-Ig	Self-made	N/A
MonoCTLA4-Ig	Self-made	N/A
CD28-Fc	Self-made	N/A
PD-1-Fc	Absolute Antibody	Cat#Pr00152–1.9
Lulizumab Pegol	ProSci	Cat#10-664
Brefeldin A	Thermo Fisher	Cat#00-4506-51
Monensin	Thermo Fisher	Cat#00-4505-51
SYTOX Blue	Thermo Fisher	Cat#S34857
Propidium Iodide	Thermo Fisher	Cat#P3566
CellTrace Far Red	Thermo Fisher	Cat#C34572
CellTrace CFSE	Thermo Fisher	Cat#C34554

(*Continued on next page*)

Continued

REAGENT or RESOURCE	SOURCE	IDENTIFIER
Critical commercial assays		
Intracellular Fixation and Permeabilization Buffer Set	Thermo Fisher	Cat#88-8824-00
CD3 MicroBead positive selection	Miltenyi Biotec	Cat#130-097-043
Experimental models: Cell lines		
CHO	Puck and Fisher[63]	N/A
RAW264.7	Raschke et al.[64]	N/A
Expi293	Thermo Fisher	Cat#A14527
Freestyle™ 293-F	Thermo Fisher	Cat#R79007
Experimental models: Organisms/strains		
Mouse: C57BL/6J wild type	WEHI	N/A
Mouse: DBA/1	WEHI	N/A
Oligonucleotides		
Ren.713 shRNA sequence: TGCTGTTGACAGTGAGCGCAG GAATTATAATGCTTATCTATAG TGAAGCCACAGATGTATAGATAA GCATTATAATTCCTATGCCTAC TGCCTCGGA	Fellmann et al. [65]	N/A
PD-L1.1684 shRNA sequence: TGCTGTTGACAGTGAGCGCCA GGATAGAATTTGTCGTTAATAGT GAAGCCACAGATGTATTAACGAC AAATTCTATCCTGATGCCTACT GCCTCGGA	Fellmann et al. [65]	N/A
CD80.598 shRNA sequence: TGCTGTTGACAGTGAGCGCCA GCTGTGTCGTTCAAAAGAATAG TGAAGCCACAGATGTATTCTTTT GAACGACACAGCTGTTGCCTA CTGCCTCGGA	Fellmann et al. [65]	N/A
CD80.1069 shRNA sequence: TGCTGTTGACAGTGAGCGCC AGAAGCTGTTTCAGAAGAAATA GTGAAGCCACAGATGTATTTCT TCTGAAACAGCTTCTGTTGCC TACTGCCTCGGA	Fellmann et al. [65]	N/A
Recombinant DNA		
MSCV-IRES-BFP	Self-made	N/A
MSCV-PGK-Puro	Clontech	N/A
MSCV-IRES-mCherry	Self-made	N/A
LTR-miR-E-NeoR-mCherry	Fellmann et al. [65]	N/A
Software and algorithms		
FlowLogic	Inivai Technologies	N/A
Prism	GraphPad	N/A
PyMOL	Schrödinger, Inc.	N/A
ASTRA 8.0.1.21 software	Wyatt Technology	N/A
Other		
BD LSRII	BD Biosciences	N/A
BD LSRFortessa	BD Biosciences	N/A
BD Influx	BD Biosciences	N/A
BD FACSAria	BD Biosciences	N/A

EXPERIMENTAL MODEL AND STUDY PARTICIPANT DETAILS

Cells were cultured at 37°C in a 10% CO_2 incubator in medium containing 100 U/mL penicillin, 100 μg/mL streptomycin (Gibco), and 10% FCS (Sigma-Aldrich). CHO cells were cultured in α-Minimal Essential Medium (α-MEM; Gibco), 293T and RAW264.7 cell lines were cultured in Dulbecco's Modified Eagle Medium (DMEM; Gibco), and both human T cells and primary mouse splenocytes were cultured in Roswell Park Memorial Institute 1640 Medium (RPMI 1640; Gibco). Freestyle 293-F cells (Thermo Fisher Scientific) were grown at 37°C, 8% CO2, 130 rpm to a density of 2×10^6/mL in FreeStyle 293 expression medium.

Wild type C57BL/6J primary mouse splenocytes stimulated *ex vivo* were of both male and female and between 12 weeks and 6 months old without appreciable differences in results.

CIA expeirments were performed with both male and female DBA/1 mice under 12 weeks old. DBA/1 mice were obtained from Walter and Eliza Hall Institute of Medical Research (WEHI) Animal Supplies and housed in standard conditions in the WEHI Animal Facility. Procedures were approved by the WEHI Animal Ethics Committee.

Consenting blood donors were healthy controls enrolled in a low-risk ethics study to examine blood leukocyte subset analysis (Monash University 2020–26385 and 2022–35867) in accordance with the principles of the Declaration of Helsinki and approved by the Monash University Human Research Ethics Committee (MUHREC).

METHOD DETAILS

Surface protein vector cloning

Mouse or human cDNA was prepared using a Verso cDNA Synthesis Kit (Thermo Fisher Scientific). Open reading frames were PCR amplified using Q5 High Fidelity DNA Polymerase (New England BioLabs). Primers incorporated EcoRI or XhoI restriction sites allowing directional cloning into MSCV-IRES-eBFP2. The following primer sequences were used, based on the indicated transcript variants:

mCD80 (NM_001359898.1):

forward 5′-TTCTCTAGGCGCCGGAATTCGCCACCATGGCTTGCAATTG-3′, reverse 5′-CGGAATTGATCCCGCTCGAGCTAAAGGAAGACGGTCTGTTCAGC-3'.

mPD-L1 (NM_021893.3):

forward 5′-TGTATCGAATTCATGAGGATATTTGCTGGCATTATATTCACAGCC -3′, reverse 5′-TCTATCCTCGAGTTACGTCTCCTCGAATTGTGTATCATTTCGG-3'.

hCD80 (NM_005191.3):

forward 5′-ATTACAGAATTCGCCACCATGGGCCACACACG-3′, reverse 5′-CTGAGACTCGAGTTATACAGGGCGTACACTTTCC-3'.

hPD-L1 (NM_014143.3):

forward 5′-TAAGCAGAATTCGCCACCATGAGGATATTTGCTGTCTTTATATTC-3′, reverse 5′-TAAGCACTCGAGTTACGTCTCCTCCAAATGTGTATC-3'.

hPD1 (NM_005018.2):

forward 5′-TAAGCAGAATTCGCCACCATGCAGATCCCCACAGGCG-3′, reverse 5′-TAAGCACTCGAGTCAGAGGGGCCAAGAG-3'.

hCD28 (NM_006139.3):

forward 5′-TAAGCAGAATTCGCCACCATGCTCAGGCTGCTCTTG-3′, reverse 5′-CCTGTACTCGAGTCAGGAGCGATAGGCTGC-3'.

hCTLA4 (NM_005214.4 with SNP rs231775 in signal peptide):

forward 5′-GTTCTAGAATTCGCCACCATGGCTTGCCTTGGATTTC-3′, reverse 5′-CCTGTACTCGAGTCAATTGATGGGAATAAAATAAGGCTGAAATTG-3'.

mCD80 and hCTLA4^{Y201A} were cloned into MSCV-IRES-eBFP2 using NEBuilder HiFi DNA Assembly (New England BioLabs), with the Y201A mutation introduced in the PCR primers. All vectors were sequence verified against the NCBI Reference Sequence Database. Sequences encoding membrane-bound anti-human CD3 single chain antibody fragment (OKT3-scFv) were based on the previously described CD5L-OKT3-scFv-CD14 sequence[66,67] (NCBI GenBank HM208750.1). Its human codon optimised open reading frame was ordered as a gBlock (Integrated DNA Technologies) and cloned into MSCV-IRES-mCherry using NEBuilder HiFi DNA Assembly (New England BioLabs).

Fluorescent fusion protein vector cloning

CD80mCherry was generated by fusing full length hCD80 (NP_005182.1) residues 1–288 to a Gly/Ser linker (2 x SGGGG) followed by monomeric mCherry.[68] A XhoI restriction site encoding Leu-Glu was included between the C terminus of hCD80 and the first Ser of the linker. PD-L1mGFP was generated by fusing full length hPD-L1 (NP_054862.1) residues 1–290 to the same Gly/Ser linker, with the same intervening XhoI site, followed by monomeric mEGFP.[69] Sequences encoding both fusion proteins were cloned into MSCV-Puro.

Recombinant antibody and Ig fusion protein vector cloning

The sequences for all recombinant antibodies and Ig fusion proteins generated in-house were cloned into XhoI/BglII digested pCAGGS using NEBuilder HiFi DNA Assembly (New England BioLabs). Ig fusion protein vectors incorporated a consensus Kozak

translation initiation sequence upstream of the human oncostatin M signal peptide[15] (residues 1–25 of NP_065391.1) followed by human CTLA4 or PD-L1 ectodomain sequences, human IgG1 Fc sequences, and a C-terminal FLAG tag. MonoCTLA4-Ig includes residues 37–174 of the soluble sCTLA4 isoform (NP_001032720.1) and both dimCTLA4-Ig and CTLA4^{HA}-Ig includes residues 37–161 of the transmembrane CTLA4 isoform (NP_005205.2). PD-L1-Fc includes residues 19–238 of the full length isoform (NP_054862.1). DimCTLA4-Ig sequences were ordered as a gBlock (Integrated DNA Technologies), modifying codons within the IgG1 hinge region to reduce G/C content. All CTLA4-Ig variants include a single Gln residue between the last residue of the CTLA4 ectodomain and the first residue of the IgG1 hinge as described for abatacept.[15] CTLA4^{HA}-Ig (MEDI5265) incorporates 8 mutations (I53R, A61T, S62N, G64S, L95A, S107A, M122Q, K130Q) that enhance binding affinity to CD80 and CD86.[51] MonoCTLA4-Ig and dimCTLA4-Ig include human IgG1 residues Glu216-Gly446 (IgG1 numbering as previously described[70]) with IgG1 hinge domain C220S, C226S, and C229S mutations as described for abatacept[15] and a monoFc region including S364N, Y407N, and K409T mutations that promote N-glycosylation and prevent Fc dimerization.[55,71] An IgG1 P238S substitution was also introduced to match abatacept protein sequence. FlexCTLA4-Ig variants were generated by inserting flexible linker peptides between Ile117 and Asp118 of CTLA4, where the soluble and transmembrane CTLA4 isoforms diverge (Figures 5C and S6D). To generate FlexCTLA4-Ig variants with varying Gly/Ser linker lengths, a gBlock was designed to encode the longest linker (6 x GGGGS repeats) but incorporating different modified codons within each GGGGS repeat to allow subsequent PCR amplification of fragments encoding shorter linkers (5 x GGGGS, 4 x GGGGS, etc). PCR products were cloned into pCAGGS using NEBuilder HiFi DNA Assembly (New England BioLabs) as described above. FlexCTLA4-Ig variants and their matched control CTLA4-Ig contain human IgG1 with a C220S mutation (IgG1 numbering as previously described[70]) but with other IgG1 hinge residues Cys226 and Cys229 intact to promote Fc dimerization. Since these cysteines were reinstated in the Flex(n)CTLA4-Ig variant series to ensure covalent homodimerisation, Ig fusion proteins for *in vivo* use harbored "LALA-PG" point mutations (human IgG1 L234A, L235A, P329G) that abrogate Fc receptor binding.[58] The TKMF5 and TKMG48 antibody variable sequences were obtained from patent US20220025051. Antibody heavy chain variable sequences were ordered as gBlocks with a human IgG1 signal peptide (MKHLWFFLLLVAAPRWVLS) and cloned into human IgG1 heavy chain constant region with LALA-PG point mutations. Antibody light chain variable sequences were ordered as gBlocks with human kappa light signal peptide (MRVPAQLLGLLLLWLPGARC) and human kappa light constant region. The CD28-antagonist PV1 antibody variable sequences were obtained from patent WO2002047721A1. The construct was designed as a monovalent single chain Fragment variable antibody (scFv) with a human kappa light signal peptide (MRVPAQLLGLLLLWLPGARC), followed by light variable sequence, $(G_4S)_3$, heavy variable sequence, GTGS linker, and 6His tail for purification as previously described.[59]

Protein expression and purification

CTLA4Ig fusions: Freestyle 293-F cells (Thermo Fisher Scientific) were grown at 37°C, 8% CO_2, 130 rpm to a density of 2×10^6/mL in FreeStyle 293 expression medium, and transiently transfected with plasmid DNA and polyethyleneimine (PEI) at a 3:1 PEI:DNA ratio (1 mg DNA per L). Cells were grown for 7 days after transfection, supplemented with Glutamax (Thermo Fisher Scientific), 0.2 mM butyric acid (Sigma–Aldrich) and 5 g/L lupin (Solabia) 1 and 4 days after transfection. Secreted recombinant protein was purified from the supernatant using Protein G resin (Cytiva). Protein was concentrated and applied to a Superdex 200 size exclusion column (Cytiva) equilibrated in DPBS (Gibco). Purest fractions as judged by non-reducing SDS-PAGE were combined, concentrated to 2 mg/mL, filter sterilised and stored at −80°C. Endotoxin was quantitated using the turbidimetric method and confirmed to be < 0.1 EU/mL for all preparations.

Antibodies: Expi293F cells (Thermo Fisher Scientific) were grown at 37°C, 8% CO_2, 130 rpm to a density of 3×10^6/mL in Expi293 expression medium, and transiently transfected with plasmid using Expifectamine (Thermo Fisher Scientific). Secreted recombinant TKMF5 and TKMG48 were purified as for CTLA4Ig fusions. CD28-antagonist PV1 antibody was captured from supernatant using Ni-NTA (Roche) and eluted using standard conditions. Eluate was concentrated and applied to a Superdex 200 size exclusion column (Cytiva) equilibrated in DPBS (Gibco). Purest fractions as judged by non-reducing SDS-PAGE were combined, concentrated to 2 mg/mL, filter sterilised and stored at −80°C. Endotoxin was quantitated using the turbidimetric method and confirmed to be < 0.1 EU/mL for all preparations.

Size-exclusion chromatography – Multi-angle light scattering (SEC-MALS)

Size exclusion chromatography of proteins at 1.3 mg/mL was performed using a Superdex 200 Increase 10/300 GL column (Cytiva) in PBS at 25°C. This was coupled to a DAWN multi-angle light scattering detector with eighteen angles and a 659 nm laser beam alongside an Optilab T-rEX refractometer (Wyatt Technology). Data collection and analysis were performed using ASTRA 8.0.1.21 software (Wyatt Technology). The refractive index of the solvent was set to 1.331, and the viscosity was set to 0.8945 cP, which are standard parameters for PBS buffer at 659 nm. The dn/dc (refractive index increment) value for all samples was defined as 0.185 mL/g.

Commercial recombinant Fc fusion proteins

The following laboratory grade mouse Fc fusion proteins were used: mCTLA4-Fc (mouse IgG1, Absolute Antibody), mPD-1-Fc (mouse IgG2a, Absolute Antibody), mCD28-Fc (human IgG1-6His, Sino Biological). The following commercial human Fc fusion proteins were used: CTLA4-Fc (human IgG1, Absolute Antibody), PD-1-Fc (mouse IgG2a, Sapphire Bioscience). Clinical grade abatacept (Bristol-Myers Squibb) was used.

Cell culture

Cells were cultured at 37°C in a 10% CO2 incubator in medium containing 100 U/mL penicillin, 100 μg/mL streptomycin (Gibco), and 10% FCS (Sigma-Aldrich). CHO cells were cultured in α-Minimal Essential Medium (α-MEM; Gibco), 293T and RAW264.7 cell lines were cultured in Dulbecco's Modified Eagle Medium (DMEM; Gibco), and both primary human T cells and primary mouse splenocytes were cultured in Roswell Park Memorial Institute 1640 Medium (RPMI 1640; Gibco). Cells were detached for passaging or harvest with Trypsin-EDTA (Gibco). For retrovirus production, expression and packaging vectors were introduced into 293T cells by calcium phosphate transfection, and retroviral transduction of CHO cells was performed using standard protocols. Primary mouse splenocytes were treated with 1 μg/mL LPS (Thermo Fisher).

Cell-cell interaction assays

Cells were harvested using TrypLE Express Dissociation Reagent (Gibco), before staining with 1.5 μM of either Cell Trace Far Red (CTFR) or carboxyfluorescein succinimidyl ester (CFSE) following manufacturer protocols. Following staining, 1.5 x 10^5 cells from each stained population were incubated together in a 96 well U-bottom plate in a final volume of 200 μL of interaction assay buffer comprising 10% (v/v) heat-inactivated FCS, 50 μM EDTA, and 1% (v/v) HEPES in PBS. For assays using CD28 or CTLA4 expressing cells, 1 x 10^5 unlabelled, CFSE and CTFR cells each were incubated together in a 96 well plate. Where required, blocking antibodies were immediately added to combined cells: either 50 μg/mL anti-hCD28 (clone TGN1412), 0.625 μg/mL ipilimumab (Bristol-Myers Squibb) or 0.5 μg/mL nivolumab (Bristol-Myers Squibb). The Fc fusion proteins abatacept, hCTLA4-Fc, or CD28-Fc were added concurrently at 50 μg/mL. For cell-cell interaction assays, cells were spun at 20*g* for 1 min, before incubating at 37°C, 10% CO_2 for 45 min. Cells were analyzed on an LSR Fortessa (BD Biosciences) using the High Throughput Sampler with acquisition settings of 0.5 μL/s sample flow rate, 100 μL sample and mixing volume, 50 μL/s mixing speed, and 2 mixes per sample. For co-culture experiments, stained cells were incubated together in the presence of the relevant blocking Abs, as well as either anti-hPD-L1-PE (0.5 μg/mL, clone MIH1) or hPD-1-Fc (100 μg/mL) and anti-mIgG2a-APC or -PE-Cy7 (50 μg/mL). Cells were incubated together at 37°C and 10% CO_2 for 45 min and analyzed on either LSR II or LSR Fortessa instruments (BD Biosciences).

RAW264.7 cell knockdown

RAW264.7 cells were retrovirally transduced with the LENC (LTR-miR-E-NeoR-mCherry) retroviral vector[65] stably express microRNA-based shRNAs targeting mPD-L1 (mPD-L1.1684), mCD80 (mCD80.598 and 1069), or negative control *Renilla* luciferase (Ren.713).

Flow cytometry of cultured cells

Harvested cells were washed with PBS. To assess binding of fusion proteins, cells were incubated with 50 μL of 10 μg/mL fusion protein for 20 min on ice unless otherwise stated, washed and then stained with 50 μL of the relevant anti-Fc secondary antibody for a further 20 min on ice. Antibodies against other antigens including free PD-L1 were only included in the secondary stain. After washing to remove excess fusion protein and antibody, cell pellets were resuspended in 100 μL of FACS buffer (PBS with 10% FCS). Flow cytometry was performed on viable cells (based on SSC/FSC, SYTOX Blue dead cell stain (Thermo Fisher), or propidium iodide (Thermo Fisher)) using a BD LSRII or LSRFortessa (BD Biosciences), and cell sorting was performed using a BD Influx or BD FACSAria (BD Biosciences) with a 100 μm nozzle. Mouse antigens were detected using the following antibodies: mPD-L1-PE-Cy7 (clone MIH5, Thermo Fisher), mPD-L1-AF647 (clone MIH6, Bio-Rad), mPD-L1-BV605 (clone MIH6, BioLegend), mCD80-APC (clone 16-10A1, Thermo Fisher), mCD11c-FITC (clone HL3, BD Biosciences), mCD11b (clone M1/70, BD Biosciences), mI-A/I-E-PE (clone M5/114.15.2, BioLegend), mCD8a-BV421 (clone 53–6.7, BioLegend). Human antigens were detected using the following antibodies: PD-L1-PE (clone MIH1, Thermo Fisher), CD80-BV711 (clone L307.4, BD Biosciences), CD28-PerCP-Cy5.5 (clone CD28.2, BioLegend), CD4-BV711 (clone SK3, BioLegend), and IL-2-PE (clone MQ1-17H12, BioLegend). MIH1 and MIH6 staining times and concentrations were optimised for selective staining of free PD-L1 only. Human CTLA4 was detected with ipilimumab directly conjugated to CF647 using Mix-*n*-Stain CF647 antibody labeling kit (Merck). Human PD-1 was detected with nivolumab directly conjugated to CF488A using Mix-*n*-Stain CF488A antibody labeling kit (Merck). Binding of unconjugated human IgG1 antibodies and Ig protein fusions was detected using an anti-human IgG1-APC secondary (clone IS11-12E4.23.20, Miltenyi Biotec). Binding of mouse IgG1 Ig protein fusions was detected using an anti-mouse IgG1-APC secondary (clone RMG1-1, BioLegend). Binding of mouse IgG2a Ig protein fusions was detected using an anti-mouse IgG2a-PE-Cy7 secondary (clone m2a-15F8, Thermo Fisher).

CD80mCherry:PD-L1mGFP population analysis

At least 250,000 mCherry/mGFP double-positive cells were recorded by flow cytometry. mCherry, mGFP, and free PD-L1 MIH1 MFI values for double-positive events were exported. Assuming a 1:1 infection, mCherry and mGFP MFI values were independently normalised against the average of all double-positive events, then mCherry:mGFP ratio was determined for each event. MIH1 MFI and the $\log_2$(mCherry:mGFP ratio) for each event was transferred into a Pivot Table. The average MIH1 MFI was determined for events grouped in intervals of 0.1–0.2 $\log_2$(mCherry:mGFP ratio). Fold changes were determined for untreated and treated samples. To generate clones, CD80mCherry:PD-L1mGFP cells were sorted based on a tight gate of PD-L1mGFP expression followed by gating

for 10 incremental degrees of CD80mCherry expression. 48 cells were sorted into individual 96-well plate wells per increment of CD80mCherry expression, and 26 of the resulting clones were screened for an equivalently high level of PD-L1mGFP expression and an even spread of CD80mCherry expression.

Cell dissociation assay

cis-CD80:PD-L1 Clone 12 cells were stained with 20 μL of 10 μg/mL fusion protein for 20 min. Following washing, cells were resuspended in 4 mL of media and incubated at 37°C and 10% CO_2 for various periods. Cells were then pelleted to remove media and stained with anti-human IgG1 as per flow cytometry staining protocols.

Primary human T cell assays

Consenting blood donors were healthy controls enrolled in a low-risk ethics study to examine blood leukocyte subset analysis (Monash University 2020–26385 and 2022–35867) in accordance with the principles of the Declaration of Helsinki and approved by the Monash University Human Research Ethics Committee (MUHREC). T cells were purified (>95%) from thawed PBMCs by MACS cell separation using human CD3 MicroBeads (Miltenyi Biotec). 100,000 T cells/well were seeded in a 12-well plate pre-seeded with 150,000 of the indicated CHO aAPC cells. Cells were co-cultured in 2 mL RPMI with 20% FCS and penicillin/streptomycin. After 4 days, cells from each co-culture were harvested and distributed into separate wells for each treatment condition on a 96-well plate pre-seeded with another 30,000 CHO aAPC cells. In 100 μL co-cultures cells were treated with 50 μg/mL CTLA4-Ig, FlexCTLA4-Ig variants, TKMF5, nivolumab, or 7.5 μg/mL lulizumab (ProSci) as indicated in Figures 4E–4J and 6F. After 4 h, each well is treated with 3 μg/mL Brefeldin A (Thermo Fisher) and 2 μM monensin (Thermo Fisher) for a further 4 h. At harvest, T cells are stained with antibodies against CD4 and PD-1, and undergo fixation and permeabilization for intracellular IL-2 staining. T cell activation was assessed by IL-2 expression.

Collagen induced arthritis (CIA) mouse model

Collagen induced arthritis was induced as previously described.[72] Briefly, DBA/1 mice aged 8–12 weeks were obtained from Walter and Eliza Hall Institute of Medical Research (WEHI) Animal Supplies and housed in standard conditions in the WEHI Animal Facility. Procedures were approved by the WEHI Animal Ethics Committee. Mice were immunized intradermally with chicken collagen type II (CII) (2 mg/mL; Sigma-Aldrich) emulsified in an equal volume of Freund's complete adjuvant (CFA) containing 5 mg/mL heat-killed *Mycobacterium tuberculosis* H37RA (Difco) on day 0. Mice received a booster intradermal injection of CII emulsified in incomplete Freund's adjuvant (IFA) on day 21. At 4 days after booster immunization prior to the onset of arthritis, mice were randomly assigned to receive intraperitoneal injection of vehicle (PBS) or 100 μg fusion proteins and/or antibodies with the indicated schedule. Clinical assessment for each paw used the following scoring system: 0, no edema/erythema; 1, inflamed digits; 2, mild edema/erythema over one surface of paw; 3, edema/erythema involving the entirety of paw; and 4, edema/erythema involving the entirety of paw and joint ankylosis. Scores were added for all four paws to generate a composite score (maximum score 16). Mice were considered to have arthritis when two consecutive positive evaluations were obtained. Where swelling was restricted to digits, the maximum score for the affected limb was 1, regardless of severity.

QUANTIFICATION AND STATISTICAL ANALYSIS

Analyses of statistical significance were determined using GraphPad Prism 10.2.0. Details of the statistical tests used, the number of replicates, and confidence intervals shown are indicated in the figure legends. Significance was defined as $p < 0.05$.